이학석사 학위논문

Probing Cosmology with Drifting Coefficient of the Field Cluster Mass Function

고립은하단 질량함수의 표류계수를 통한 우주론 탐구

2022년 8월

서울대학교 대학원

물리·천문학부 천문학전공

유 수 호

Probing Cosmology with Drifting Coefficient of the Field Cluster Mass Function

고립은하단 질량함수의 표류계수를 통한 우주론 탐구

지도교수 이 정 훈

이 논문을 이학석사 학위논문으로 제출함

2022년 4월

서울대학교 대학원

물리·천문학부 천문학전공

유 수 호

유 수 호의 이학석사 학위논문을 인준함

2022년 7월

위 원 장 ______________________________

부 위 원 장 ______________________________

위 원 ______________________________

Probing Cosmology with Drifting Coefficient of the Field Cluster Mass Function

by

Suho Ryu
(shryu@astro.snu.ac.kr)

A dissertation submitted in partial fulfillment of the requirements for the degree of

Master of Science

in

Astronomy

in

Astronomy Program
Department of Physics and Astronomy
Seoul National University

Committee:

Professor Myungshin Im

Professor Jounghun Lee

Professor Ho Seong Hwang

ABSTRACT

The collapse barrier, δ_c, of the field clusters located in the low-density environment is deterministic rather than diffusive, unlike that of the wall counterparts located in the superclusters. Analyzing the data from the Mira-Titan (dynamical dark energy cosmology) and CoDECS (coupled dark energy cosmology) simulations we investigate the evolution of deterministic collapse barrier on non-standard dark energy models. We also use Cosmological Massive Neutrino (massive neutrinos cosmology) and DUSTGRAIN-*pathfinder* ($f(R)$ gravity and $f(R)$ gravity with massive neutrinos) simulations to study various non-standard cosmologies. We first numerically determine mass functions of the field clusters at various redshifts for each cosmology. Then, we compare the numerical mass functions with the analytical formula characterized by a single parameter called the drifting coefficient, $\beta(z)$, which quantifies the drifts of the collapse barrier from the Einstein-de Sitter spherical value, $\delta_{sc} = 1.686$. It is found that the analytic formula with the best-fit coefficient excellently interpret the numerical results at all redshifts for all of the cosmologies. Regardless of the background cosmology, the $\beta(z)$ exhibits a universal behavior of having a positive value at $z = 0$ but gradually converging down to zero as the dominance of dark energy fades with the increment of z. A significant difference of critical redshift z_c, at which $\beta(z = z_c) = 0$, is found among different cosmologies distinguishing even the degenerate cosmologies with almost identical power spectrum and cluster mass functions. It is concluded that the evolution of the departure from the spherically symmetric collapse measured by $\beta(z)$ is a powerful probe of cosmology.

Keywords: Large-scale structure − Cosmological models

Student Number: 2020-25868

Papers Included in this Thesis:

Ryu, S. & Lee, J. 2020, ApJ, 889, 62
Evolution of the Deterministic Collapse Barrier of the Field Clusters as a Probe of Cosmology

Ryu, S. & Lee, J. 2020, ApJ, 894, 65
Constraining the Neutrino Mass with the Drifting Coefficient of the Field Cluster Mass Function

Ryu, S., Lee, J., & Baldi, M. 2020, ApJ, 904, 93
Breaking the Dark Degeneracy with the Drifting Coefficient of the Field Cluster Mass Function

Contents

List of Figures

List of Tables

Chapter 1

Introduction

[1] Ever since Press & Schechter (1974) derived an analytic formula for the cluster mass function based on the excursion set theory, its power and usefulness as a cosmological probe has been widely demonstrated and well appreciated in the field of the large scale structure (e.g., Fan et al. 1997; Wang & Steinhardt 1998; Vikhlinin et al. 2009; Basilakos et al. 2010; Ichiki & Takada 2012; Benson et al. 2013; Planck Collaboration et al. 2014). The excursion set theory basically depicts the gravitational growth and collapse of an over-dense region into a bound object as a *random walk process* confined under a barrier whose height is determined by the underlying dynamics. In the original formulation of Press & Schechter (1974) who adopted the spherical dynamics, the height of the collapse barrier has a constant value, δ_{sc}, being independent with the cluster mass. Various N-body experiments, however, revealed that the original Press-Schechter mass function failed to match well the numerical results at quantitative levels, implying the inadequacy of the spherical dynamics (Bond & Myers 1996, and references therein).

In the subsequent works which employed more realistic ellipsoidal dynamics to an-

[1] This chapter was published in Ryu, S. & Lee, J. 2020, ApJ, 889, 62; Ryu, S. & Lee, J. 2020, ApJ, 894, 65; Ryu, S., Lee, J., & Baldi, M. 2020, ApJ, 904, 93.

alytically derive the excursion set mass function, the height of the collapse barrier was deemed no longer a constant value but a decreasing function of the cluster mass, M, to account for the fact that the collapse process deviates further from the spherical dynamics on the lower mass scales (e.g., Bond & Myers 1996; Sheth et al. 2001; Chiueh & Lee 2001; Sheth & Tormen 2002). Although better agreements with the numerical results were achieved by employing the mass-dependent ellipsoidal collapse barrier, the purely analytic evaluation of the cluster mass function had to be relinquished on the ground that no unique condition for the ellipsoidal collapse exists unlike the case of the spherical collapse (Bond & Myers 1996; Chiueh & Lee 2001; Sheth et al. 2001). It was required to empirically determine the functional form of the ellipsoidal collapse barrier height by fitting the analytic formula to the numerical results, which in turn inevitably weakened the power of the cluster mass function as a probe of cosmology. Besides, the high-resolution N-body simulations revealed that even on the fixed mass scale the collapse barrier height exhibited substantial variations with the environments as well as with the cluster identification algorithms (e.g., Robertson et al. 2009, and references therein). These numerical findings casted down an excursion set based analytic modeling of the cluster mass function, leading the community to acquiesce in relying on mere fitting formulae with multiple adjustable parameters (e.g., Tinker et al. 2008).

The excursion set modeling of the cluster mass function, however, attracted a revived attention when Maggiore & Riotto (2010a,b) brought up an insightful idea that the collapse barrier height should be treated as a stochastic variable rather than a deterministic value. Ascribing the diffusive scatters of the collapse barrier height to the incessant disturbing influence from the surrounding on the clusters, Maggiore & Riotto (2010a) successfully incorporated the concept of the stochastic barrier height into the excursion set theory with the help of the path integral method and showed that the accuracy of the generalized excursion set mass function with stochastic collapse barrier was considerably improved even though it has only a single parameter, D_B, which measures the degree of the stochasticity of δ_c whose ensemble average coincides with δ_{sc}.

Corasaniti & Achitouv (2011a, hereafter, CA) derived a more accurate mass function by extending the formalism of Maggiore & Riotto (2010a) to the ellipsoidal collapse case where the ensemble average, $\langle\delta_c\rangle$, does not coincide with δ_{sc} but drifts away from it, depending on the cluster mass scale. As a trade-off of introducing an additional parameter, β, to quantify the deviation of $\langle\delta_c\rangle$ from δ_{sc}, Corasaniti & Achitouv (2011a) won two-fold achievement: matching the numerical results as excellently well as pure fitting formula and simultaneously providing much deeper physical understanding about the cluster abundance and its evolution (see also Corasaniti, & Achitouv 2011b). Notwithstanding, the efficacy of the generalized excursion set mass function as a cosmological diagnostics was not greatly elevated by introducing the concept of a *stochastically drifting* collapse barrier due to the obscurity in the choice of the joint probability density functions of δ_c expressed in terms of the two parameters, D_B and β (Achitouv et al. 2014, and references therein).

It was Lee (2012) who fathomed out that for the case of the field clusters embedded in the lowest-density environments the collapse barrier height would behave deterministically (i.e., $D_B = 0$) since the degree of the surrounding disturbance as well as ambiguity in the identification of the field clusters would be negligibly low in the underdense regions. Defining the field clusters as those which do not belong to superclusters, she modified the CA formalism by setting $D_B = 0$ and confirmed its validity against the N-body results at various redshifts for the case of the currently favored ΛCDM (cosmological constant Λ and cold dark matter) model. The analysis of Lee (2012) also found a clear trend that the value of β gradually dwindles away to 0 as the redshift z increases, which indicates that at some critical redshift, z_c, the deterministic collapse barrier height, δ_c, for the field clusters will become equal to δ_{sc}.

This trend may be physically understood by the following logics. The high-z field clusters correspond to the highest peaks in the linear density field whose gravitational collapse proceeds spherically (Bernardeau 1994). At high redshifts $z > 0.7$ where the dark matter (DM) density exceeds that of dark energy (DE), the universe is well approximated by the Einstein-de Sitter (EdS) cosmology in which $\delta_{sc} = 1.686$. We speculate that since the convergence rate of the universe to the EdS model is quite susceptible to the background cosmology, the deterministic collapse barrier of the field clusters would evolve differently among different cosmologies. The aim of this Paper is to examine if the concept of the deterministic collapse barrier for the field clusters is valid even in various non-standard cosmologies and to explore whether or not the evolution of β, i.e., the deviation of the deterministic collapse barrier from the EdS spherical collapse value of $\delta_{sc} = 1.686$, can discriminate degenerate cosmologies and be used as a complementary probe of cosmology.

A cosmic degeneracy refers to the circumstance that a standard diagnostic fails to distinguish between different cosmologies with high statistical significance. For example, the cluster mass function, which is regarded as one of the most powerful probes of cosmology based on the large scale structure, is unable to discriminate a coupled dark energy (cDE) model in which a scalar field DE coupled to DM particles follows a supergravity potential (Baldi et al. 2010) from the ΛCDM cosmology. Another example, the cluster mass function fails to discriminate the effect of a low amplitude of the linear density power spectrum from that of massive neutrinos (ν) (dubbed the σ_8-$\sum m_\nu$ degeneracy) in a $\nu\Lambda$CDM (massive neutrinos ν + cosmological constant Λ + Cold Dark Matter) cosmology. Since the cosmic degeneracy is caused by the limited sensitivity of a given standard diagnostic on which the degenerate models have almost the same effects, what is required to break it is to overcome the limitation by utilizing prior information from other independent diagnostics.

The latest Planck analysis of the Cosmic Microwave Background (CMB) temperature power spectra combined with the priors from the weak gravitational lensing (WL) and Baryonic Acoustic Oscillations (BAO) concluded $M_\nu \leq 0.12\,\mathrm{eV}$ (Planck Collaboration et al. 2018), assuming the base flat ΛCDM cosmology (see also Vagnozzi et al. 2017). A higher value of M_ν above $0.12\,\mathrm{eV}$, however, can still be accommodated by the Planck data, if the assumption about the background cosmology is released (see Choudhury & Choubey 2018; Choudhury & Hannestad 2019, and references therein) or if different priors are used to complement the CMB probe (e.g., Giusarma et al. 2016). For the past decade, the cluster mass function has been prevalently promoted as an useful complementary probe of M_ν (e.g., Marulli et al. 2011; Ichiki & Takada 2012; Costanzi et al. 2013; Villaescusa-Navarro et al. 2013; Castorina et al. 2014; Biswas et al. 2019; Hagstotz et al. 2019). Although the cluster mass function is only indirectly linked to M_ν through its dependence on the linear density power spectrum, it has a practical advantage as a probe of M_ν, being more readily observable than the linear density power spectrum, the measurements of which are often plagued by the systematics stemmed from the existence of nonlinear galaxy bias (Giusarma et al. 2018, and references therein).

Due to the inherent non-sphericity and stochastic aspect of the cluster formation process that defies purely analytic modeling from the first principle, a theoretical prediction for the cluster abundance and its dependence on M_ν was conventionally made in the *empirically* modified excursion set formalism (e.g., Costanzi et al. 2013; Villaescusa-Navarro et al. 2013; Biswas et al. 2019). While a link between the cluster abundance and M_ν through the linear power spectrum is provided by the excursion set theory, the required accuracy and precision was achieved by the empirical modification of the theory, i.e., deteriorating of a physical model into a fitting formula with multiple free parameters (Warren et al. 2006; Tinker et al. 2008). Lack of a physical model for the cluster abundance undermines its power as a probe of M_ν. To make matters worse, the notorious σ_8-M_ν degeneracy of the initial density power spectrum translates into the relative low sensitivity of the cluster mass function to M_ν. Given the aforementioned difficulties in constraining M_ν with the cluster abundance, what may be desirable to have is a new probe, well described by a physical model, free from the σ_8-M_ν degeneracy, and highly sensitive to the variation of M_ν. Our goal here is to prove that the drifting coefficient of the field cluster mass function fulfills this expectation.

There are a few cosmic degeneracies which have been found more difficult to break even by combining the priors from several independent diagnostics. A notorious example is the cosmic degeneracy between the ΛCDM + GR and the νCDM + MG cosmologies, where GR and MG stand for the general relativity and modified gravity, respectively (see e.g. Baldi et al. 2014; Wright et al. 2019). All different versions of the MG theory adopt a common tenet that the apparent acceleration of the present Universe is caused not by the dominance of the anti-gravitational Λ at the present epoch but by the deviation of the gravitational law from the prediction of GR on cosmological scales. The consequence of this tenet is the existence of a long-range fifth force, which in turn has an effect of enhancing the density power spectrum on the scales comparable to those affected by the suppression due to free streaming massive neutrinos (for a review, see Clifton et al. 2012).

In the theory of $f(R)$ gravity, the gravitational dynamics is defined by a modified Einstein-Hilbert action functional to which an arbitrary function of the Ricci scalar, $f(R)$, is introduced as a substitution for the Ricci scalar R itself of the original action in GR (see e.g., Buchdahl 1970; Starobinsky 1980; Hu & Sawicki 2007). Choosing as a viable MG the $f(R)$ gravity in which the Ricci scalar term, R, in the Einstein-Hilbert action functional is replaced by an arbitrary function, $f(R)$, Baldi et al. (2014)

numerically investigated a possible cosmic degeneracy between the ΛCDM + GR and the νCDM + $f(R)$, and demonstrated that the two cosmologies cannot be discriminated from each other by several standard diagnostics such as the nonlinear density power spectra, halo bias and cluster mass functions (see also Hagstotz et al. 2019; Garcia-Farieta et al. 2019). The nonlinear growth rate functions, cluster velocity dispersions, and tomographic higher-order weak lensing statistics were proposed in subsequent works as candidate diagnostics that could be capable of breaking this cosmic degeneracy (Giocoli et al. 2019; Peel et al. 2018; Hagstotz et al. 2019), also employing Machine Learning techniques (Peel et al. 2019; Merten et al. 2019). Our goal here is to explore whether or not this new diagnostics can break other cosmic degeneracies including that between the ΛCDM + GR and the νCDM + MG models.

Chapter 2

An Analytical Model for the Isolated Cluster Mass Function

[1] The excursion set modeling of the cluster mass function relates the differential number density of the clusters, $dN/d\ln M$, to the *multiplicity function*, $f(\sigma)$, as (Reed et al. 2003)

$$\frac{d\,N(M,z)}{d\ln M} = \frac{\bar{\rho}}{M}\left|\frac{d\ln\sigma^{-1}}{d\ln M}\right| f[\sigma(M,z)]\,, \tag{2.1}$$

where $\bar{\rho}$ is the mean matter density at the present epoch, and $\sigma(M,z)$ is the rms density fluctuation of linear density field smoothed on the mass scale M at redshift z, and $f(\sigma)$ counts the number of the randomly walking overdensities, δ, that just touch the collapse barrier, δ_c, when the underlying linear density field has the inverse of the rms fluctuation in the differential range of $[\ln\sigma^{-1},\ \ln\sigma^{-1} + d\ln\sigma^{-1}]$. The cosmology dependence of $dN/d\ln M$ stems from the dependence of $\sigma(M,z)$ on the linear growth factor, $D(z)$, and linear density power spectrum, $P(k)$ as:

$$\sigma^2(M,z) \propto D^2(z)\int_0^\infty dk\,k^2\,P(k)W^2(k,M), \tag{2.2}$$

[1]This chapter was published in Ryu, S. & Lee, J. 2020, ApJ, 889, 62.

where $W(k, M)$ is a window function. Three types of window (filter) functions are widely used in the field of cosmology: spherical top-hat filter, Gaussian filter and sharp k-space filter. We list the functional froms and their Fourier representations of the three window functions below. The 'natural volume' V_f of the window funtions are defined as the integral of $W(r)/W(0)$ over all space (Lacey & Cole 1994).

1. Top-Hat

$$W_{TH}(r) = \begin{cases} 3/(4\pi R_{TH}^3) & r < R_{TH} \\ 0 & r > R_{TH} \end{cases} \tag{2.3}$$

$$\hat{W}_{TH}(k) = \frac{3}{(kR_{TH})^3}[\sin(kR_{TH}) - (kR_{TH})\cos(kR_{TH})] \tag{2.4}$$

$$V_{TH} = (4\pi/3)R_{TH}^3 \tag{2.5}$$

2. Gaussian

$$W_G(r) = \frac{1}{(2\pi)^{3/2}R_G^3}\exp[-r^2/(2R_G^2)] \tag{2.6}$$

$$\hat{W}_G(k) = \exp[-k^2/(2R_G^2)] \tag{2.7}$$

$$V_{TH} = (2\pi)^{3/2}R_G^3 \tag{2.8}$$

3. Sharp k-space

$$W_k(r) = \frac{1}{2\pi^2 r^3}[\sin(r/R_k) - (r/R_k)\cos(r/R_k)] \tag{2.9}$$

$$\hat{W}_{TH}(k) = \begin{cases} 1 & k < 1/R_k \\ 0 & k > 1/R_k \end{cases} \tag{2.10}$$

$$V_k = 6\pi^2 R_k^3 \tag{2.11}$$

Here, we use the spherical top-hat window function for our analytical field cluster mass function model throughout the study. The linear growth factor $D(z)$ is known to have the following analytical expression for the case of ΛCDM universe (Lahav et al. 1991):

$$D(z) \propto \frac{5}{2}\Omega_m[\Omega_m(1+z)^3+\Omega_\Lambda]^{1/2}\int_z^\infty dz'\frac{1+z'}{[\Omega_m(1+z')^3+\Omega_\Lambda]^{3/2}}. \tag{2.12}$$

Here we normalize $D(z)$ to satisfy $D(z=0)=1$.

Assuming that δ_c is a stochastically drifting variable as in Maggiore & Riotto (2010a,b), the CA formalism approximates the multiplicity function by

$$f_{\rm ca}(\sigma;D_B,\beta) \approx f^{(0)}(\sigma;D_B,\beta)+f^{(1)}_{\beta=0}(\sigma;D_B)+f^{(1)}_{\beta}(\sigma;D_B,\beta)+f^{(1)}_{\beta^2}(\sigma;D_B,\beta), \tag{2.13}$$

$$f^{(0)}(\sigma;D_B,\beta) = \frac{\delta_{sc}}{\sigma\sqrt{1+D_B}}\sqrt{\frac{2}{\pi}}\,e^{-\frac{(\delta_{sc}+\beta\sigma^2)^2}{2\sigma^2(1+D_B)}}, \tag{2.14}$$

$$f^{(1)}_{\beta=0}(\sigma;D_B) = -\tilde{\kappa}\frac{\delta_{sc}}{\sigma}\sqrt{\frac{2a}{\pi}}\left[e^{-\frac{a\delta_{sc}^2}{2\sigma^2}}-\frac{1}{2}\Gamma\left(0,\frac{a\delta_{sc}^2}{2\sigma^2}\right)\right], \tag{2.15}$$

$$f^{(1)}_{\beta}(\sigma;D_B,\beta) = -\beta\, a\,\delta_{sc}\left[f^{(1)}_{\beta=0}(\sigma;D_B)+\tilde{\kappa}\,{\rm erfc}\left(\frac{\delta_{sc}}{\sigma}\sqrt{\frac{a}{2}}\right)\right], \tag{2.16}$$

$$f^{(1)}_{\beta^2}(\sigma;D_B,\beta) = \beta^2a^2\delta_{sc}^2\tilde{\kappa}\Bigg\{{\rm erfc}\left(\frac{\delta_{sc}}{\sigma}\sqrt{\frac{a}{2}}\right)+ \tag{2.17}$$

$$\frac{\sigma}{a\delta_{sc}}\sqrt{\frac{a}{2\pi}}\left[e^{-\frac{a\delta_{sc}^2}{2\sigma^2}}\left(\frac{1}{2}-\frac{a\delta_{sc}^2}{\sigma^2}\right)+\frac{3}{4}\frac{a\delta_{sc}^2}{\sigma^2}\Gamma\left(0,\frac{a\delta_{sc}^2}{2\sigma^2}\right)\right]\Bigg\}, \tag{2.18}$$

with $a\equiv 1/(1+D_B)$, $\tilde{\kappa}=\kappa a$, $\kappa=0.475$, upper incomplete gamma function $\Gamma(0,x)$ and complementary error function ${\rm erfc}(x)$. The statistical properties of the randomly drifting collapse barrier, δ_c, are described by the two parameters, D_B and β, in Equations (2.13)-(2.17). The former, called the diffusion coefficient, is related to the scatters of δ_c from its ensemble average, while the latter, called the drifting average coefficient, measures how much the ensemble average of δ_c drifts away from the deterministic height of the spherical collapse barrier δ_{sc} on a given mass scale (Corasaniti & Achitouv 2011a; Corasaniti, & Achitouv 2011b).

Lee (2012) suggested that for the case of the field clusters the collapse barrier height should be deterministic (i.e., $D_B=0$) rather than stochastic since the field clusters would experience the least disturbance from the surroundings. Setting $D_B=0$ in Equation (2.13) and putting it into Equation (2.1), she modified the CA formalism to evaluate the mass function of the field clusters, $dN_I/d\ln M$, as

$$\frac{dN_I(M,z)}{d\ln M} = \frac{\bar{\rho}}{M}\left|\frac{d\ln\sigma^{-1}}{d\ln M}\right| f_{\rm ca}\left[\sigma(M,z); D_B = 0, \beta\right], \tag{2.19}$$

which has a single coefficient, β. Empirically determining the values of β at three different redshifts ($z = 0, 0.5, 1$) through numerical adjustment process, Lee (2012) confirmed the validity of Equation (2.19) for the ΛCDM case. In the following chapters, we will test this analytic model against the numerical results from N-body simulations performed for various non-standard cosmologies, investigate how β evolves in different cosmologies and seek its potential as a new complimentary probe of cosmology.

Although the exact value of δ_{sc} has been known to weakly depend on the background cosmology as well as on the redshift (Eke et al. 1996; Pace et al. 2010), we regard δ_{sc} as a constant, setting it at the Einstein-de Sitter value of 1.686 (Gunn, & Gott 1972), as done in the original formulation of the generalized excursion set mass function theory (Maggiore & Riotto 2010a,b). In reality, the gravitational collapse proceeds in a non-spherical way, for which the actual critical density contrast, δ_c, departs from the idealistic spherical threshold, δ_{sc}. The cosmology dependence of δ_c is expected to overwhelm that of δ_{sc}, given that the degree of the non-sphericity of the collapse process is closely linked with the anisotropy of the cosmic web, which in turn possesses strong dependence on the background cosmology (e.g., Shim & Lee 2013; Naidoo et al. 2020). Unlike δ_{sc}, however, the value of δ_c and its link to the initial conditions cannot be analytically derived from first principles due to the complexity associated with the non-spherical collapse process (Bond & Myers 1996).

Chapter 3

Comparison with the Numerical Results for wCDM model

3.1 Comparison with the Numerical Results

[1] To investigate if Equation (2.19) can be validly applied to the case of a wCDM cosmology where the DE equation of state, w, evolves with time, we resort to the Mira-Titan simulation conducted by Heitmann et al. (2016) on a periodic box of $(2100\,\mathrm{Mpc})^3$ with 3200^3 DM particles of individual mass $m_{dm} \sim 10^{10}\,M_\odot$ for 10 different wCDM cosmologies (designated as M001, M002, M003, M004, M005, M006, M007, M008, M009, M010) as well as for the ΛCDM case (see also, Habib et al. 2016; Heitmann et al. 2019). The initial condition of each cosmology was specified by seven parameters, $\{\Omega_m, \Omega_b, h, \sigma_8, n_s, w_0, w_a\}$, under the common assumption of a spatially flat geometry $(\Omega_{de} + \Omega_m = 1)$, no neutrino $(\Omega_\nu = 0)$ and evolution of w given as $w = w_0 + w_a z/(1+z)$ (Chevallier & Polarski 2001; Linder 2003).

For the ΛCDM case ($w_0 = -1$, $w_a = 0$), the other five cosmological parameters

[1] This chapter was published in Ryu, S. & Lee, J. 2020, ApJ, 889, 62.

Table 3.1. Key cosmological parameters for the eleven models from the HACC simulations

Cosmology	Ω_m	Ω_b	h	σ_8	n_s	w_0	w_a
ΛCDM	0.2648	0.04479	0.7100	0.8000	0.9630	-1.0000	0.0000
M001	0.3871	0.05945	0.6167	0.8778	0.9611	-0.7000	0.6722
M002	0.2411	0.04139	0.7500	0.8556	1.0500	-1.0330	0.9111
M003	0.3017	0.04271	0.7167	0.9000	0.8944	-1.1000	-0.2833
M004	0.3642	0.06710	0.5833	0.7889	0.8722	-1.1670	1.1500
M005	0.1983	0.03253	0.8500	0.7667	0.9833	-1.2330	-0.0445
M006	0.4354	0.07107	0.5500	0.8333	0.9167	-0.7667	0.1944
M007	0.2265	0.03324	0.8167	0.8111	1.0280	-0.8333	-1.0000
M008	0.2570	0.04939	0.6833	0.7000	1.0060	-0.9000	0.4333
M009	0.3299	0.05141	0.6500	0.7444	0.8500	-0.9667	-0.7611
M010	0.2083	0.03649	0.7833	0.7222	0.9389	-1.3000	-0.5222

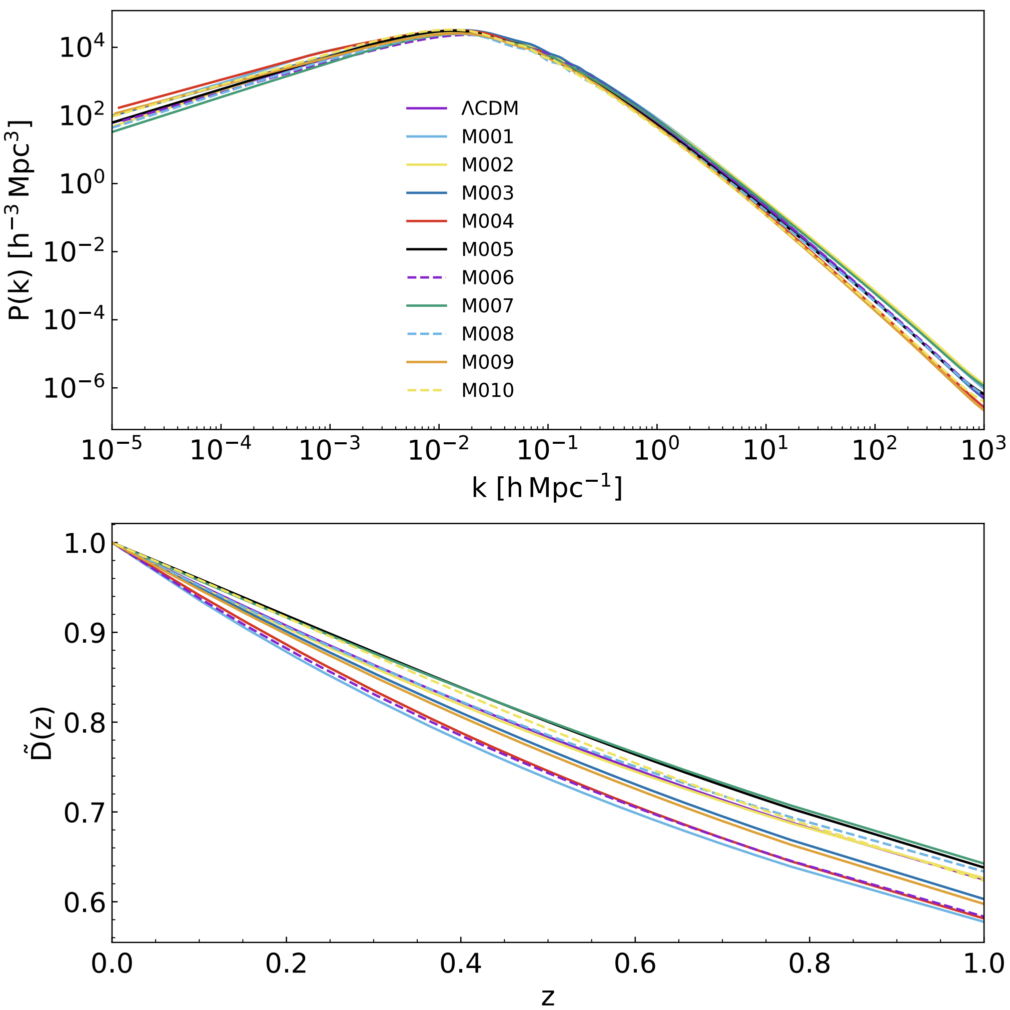

Figure 3.1. Linear density power spectra (top panel) and linear growth factors (bottom panel) from the Mira-Titan simulations for the cases of the ΛCDM and ten different dynamical wCDM cosmologies (Heitmann et al. 2016).

were set at the best-fit values from the Seven-Year Wilkinson Microwave Anisotropy Probe (WMAP7) (Komatsu et al. 2011). For the wCDM cosmologies, the values of the seven key cosmological parameters including w_0 and w_a were deliberately chosen to be in the ranges that embrace the WMAP7 constraints (for the details, see Heitmann et al. 2009, 2016). Table 3.1 lists the values of the key cosmological parameters for each of the eleven different cosmologies from the Mira-Titan simulation (see also Table 3 in Lawrence et al. 2017). Figure 3.1 plots the linear power spectra at the present epoch, $P(k)$, and the linear growth factor, $D(z)$, for the eleven cosmologies (in the top and bottom panels, respectively), computed by the CAMB code (Lewis et al. 2000). Note that the three models, M003, M005 and M008 are almost indistinguishable from the ΛCDM model in $P(k)$, while the two models, M007 and M009, yield $D(z)$ the shapes of which are very similar to that for the ΛCDM case.

Heitmann et al. (2016) compiled the catalogs of the DM halos identified by applying the friends-of-friends (FoF) algorithm with a linking length of $b_c\bar{d}_p$ with $b_c = 0.168$ and mean particle separation $\bar{d}_p$ to each particle snapshot in the redshift range of $0.0 \le z \le 4.0$. Following the same procedure of Lee (2012), we analyze the FoF halo catalogs from each Mira-Titan universe to numerically determine the mass functions of the field clusters and the associated errors as well:

1. Make a sample of the cluster halos with masses larger than $M_c = 3\times10^{13}\,h^{-1}\,M_\odot$ out of the halo catalog at a given redshift in the range of $0 \le z \le z_c \sim 1$. The catalogs at higher redshifts, $z > z_c$ are excluded from the analysis on the ground that the field clusters at $z > z_c$ are too rare to yield statistically significant results.

2. Apply to the above sample the FoF algorithm with a linking length of $b_{sc}\bar{d}_c = 2b_c\bar{d}_c$ with mean cluster halo separation $\bar{d}_c$ to find a supercluster as a cluster of clusters each of which consists of two and more cluster halos. This specific choice

of the linking length was made by Lee (2012) to guarantee that the degree of the disturbance from the surroundings on the field clusters is indeed negligible (i.e., $D_B = 0$) (see Figure 2 in Lee 2012).

3. Find the cluster halos in the sample which appertain to none of the identified superclusters as the field clusters and count them, $dN_{\rm I}$, in the logarithmic mass bin, $[\ln M, \ln M + d\ln M]$.

4. Split the field clusters into eight Jackknife subsamples according to their positions and separately determine $dN_{\rm I}/d\ln M$ from each subsample. Evaluate the Jackknife errors in the measurement of $dN_{\rm I}/d\ln M$ as one standard deviation scatter around the ensemble average over the eight subsamples.

Now that the mass functions of the field clusters from the Mira-Titan simulations are all determined, we compare them with Equation (2.19) by adjusting the single coefficient, β. For this comparison, the spherical barrier height, δ_{sc}, is set at the EdS value of 1.686, since it varies only very weakly with the back ground cosmology (e.g., Eke et al. 1996; Pace et al. 2010). We employ the χ^2-statistics to determine the best-fit value of β and estimate the associated error, σ_β, as $1/\sqrt{I_\beta}$, where I_β is the Fisher information given as $I_\beta \equiv d^2\chi^2/d\beta^2$ at the best-fit value of β, at each redshift for each cosmology.

Figure 3.2 plots the numerical result (filled circles) as well as Equation (2.19) with the best-fit value of β (red solid line) for eleven different cosmologies at $z = 0$. In each panel, the analytic mass function with the best-fit β for the ΛCDM case is shown as dashed line for comparison. Figures 3.3-3.4 plot the same as Figure 3.2 but at $z = 0.4$ and $z = 0.78$, respectively. As can be seen, Equation (2.19) with the best-fit β is quite successful in matching the numerically determined mass functions of the field clusters for all of the eleven cosmologies at all of the three redshifts. As emphasized in Lee

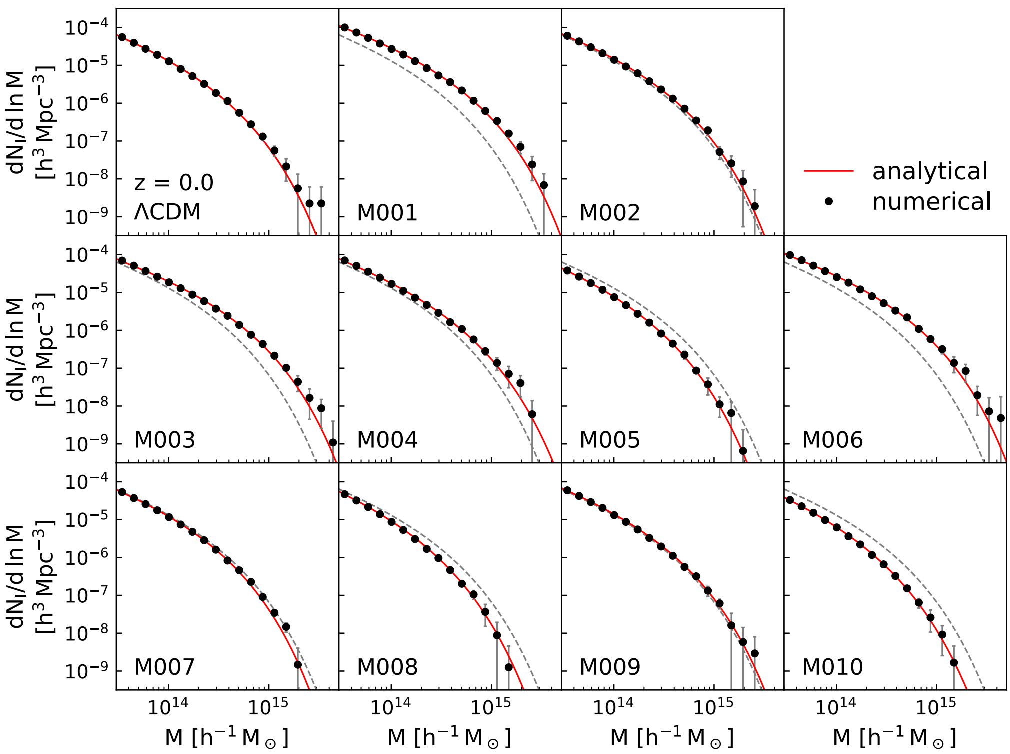

Figure 3.2. Numerically obtained mass functions of the field clusters (filled circles) compared with the analytic formula (red solid lines) for 10 different dynamical wCDM cosmologies as well as for the ΛCDM case at $z = 0$.

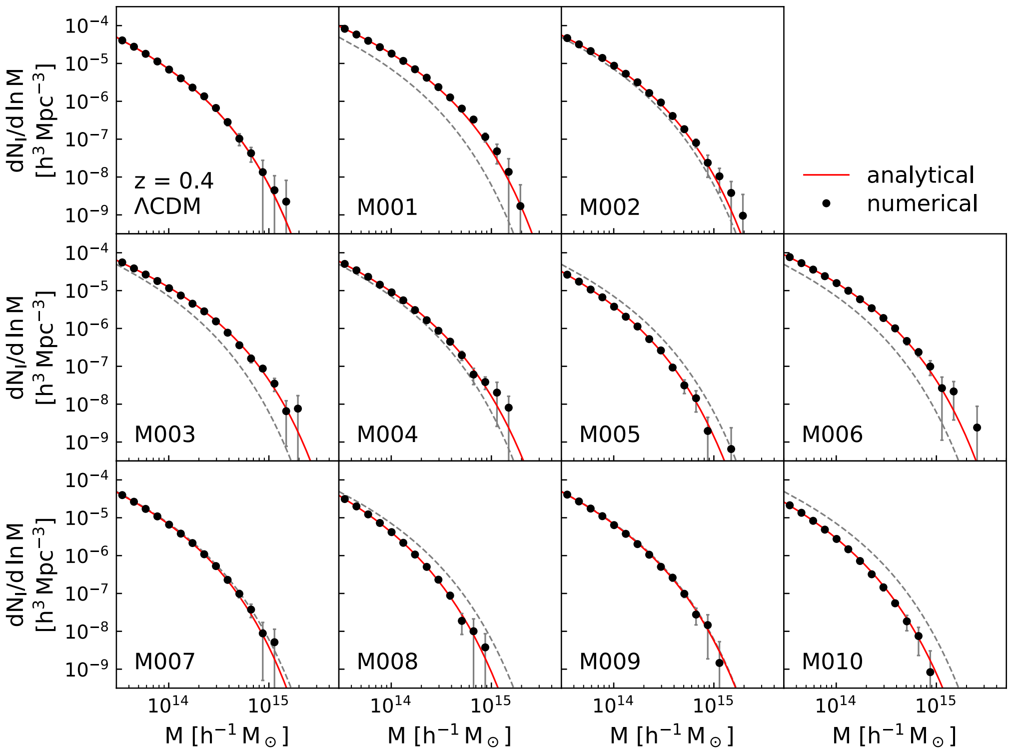

Figure 3.3. Same as Figure 3.2 but for at $z = 0.4$.

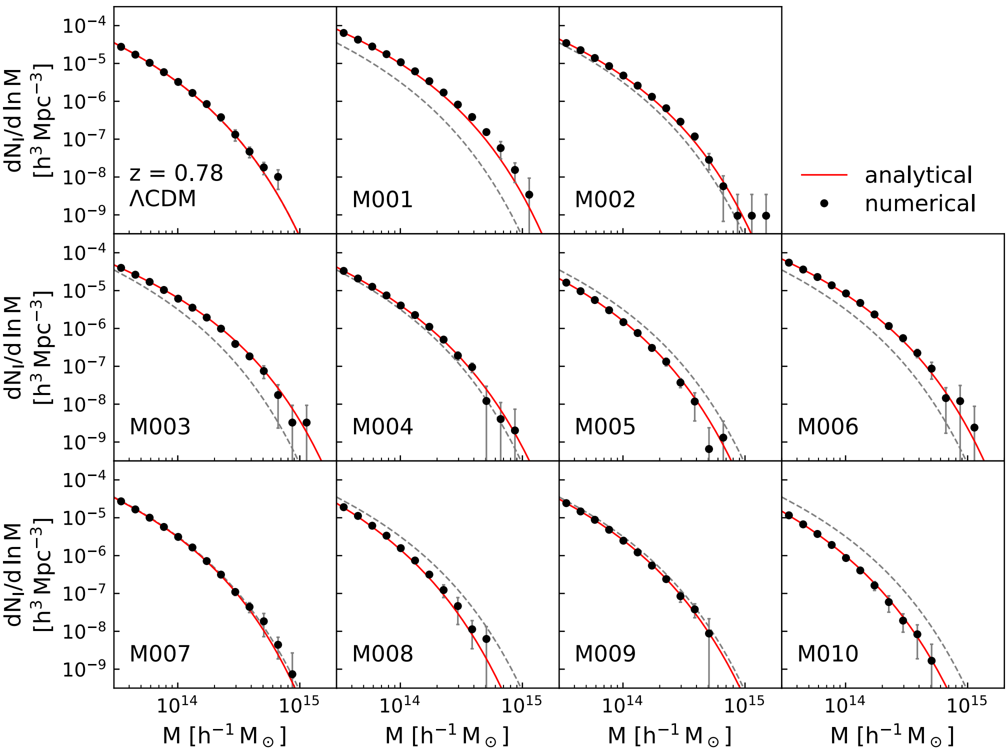

Figure 3.4. Same as Figure 3.2 but for at $z = 0.78$.

(2012), the modified CA formalism with $D_B = 0$ describes well not only the shape but also amplitude of the mass function of the field clusters even though it has only a single parameter, β. The good agreements between the analytical and numerical results shown in Figures 3.2-3.4 prove that the modified CA formalism with the deterministic collapse barrier for the field clusters can be legitimately extended to the wCDM cosmologies.

It is, however, worth mentioning here that the analytic model for the field cluster mass function, Equation (2.19), is found to be valid in the limited redshift range $z \leq z_c$, which we suspect is due to the failure of the assumption $D_B = 0$ at higher redshifts $z > z_c \sim 1$. The low abundance of the clusters with $M \geq M_c$ at $z > z_c$ makes it difficult to properly identify the superclusters via the FoF algorithm, which in turn contaminates the identification of the field clusters. In other words, the field clusters identified via the FoF algorithm at $z > z_c$ may not be isolated enough to satisfy the condition of $D_B = 0$.

3.2 Evolution of the Drifting Collapse Barrier

Figure 3.5 plots the best-fit value of β determined in Section 3.1 versus z for the eleven cosmologies, revealing the presence of a strong anti-correlation between β and z. We discover an universal behavior of $\beta(z)$ from all of the eleven cosmologies: it monotonically declines toward 0 as the redshift increases up to $z \geq 1$. In the range of $0 \leq z \leq 0.3$, it declines relatively slowly with z, while in the higher z-range it drops quite rapidly down to zero. The drifting coefficient, $\beta(z)$, from each of the eleven cosmologies is, however, manifestly different from one another in its declining rate and amplitude as well as in the critical redshift at which $\beta(z)$ becomes zero.

Although $\delta_{sc}/\sigma(M, z)$ may play a partial role to induce the cosmology dependence of $\beta(z)$, we believe that it should not be the main contribution. First of all, the spherical

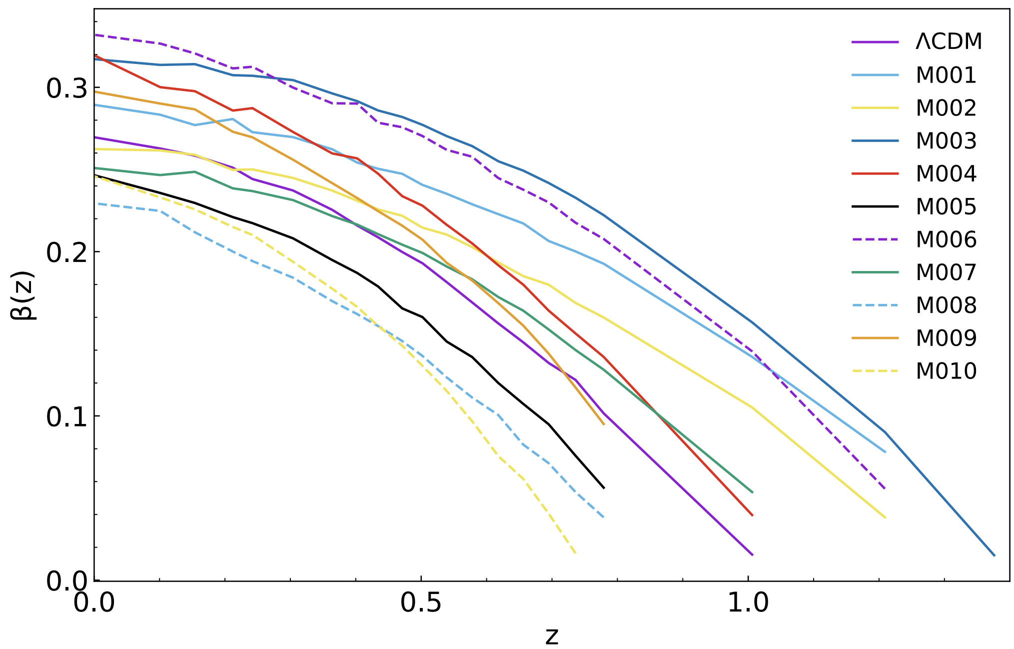

Figure 3.5. Redshift evolution of the drifting coefficient, β, for 11 different DE cosmologies.

collapse barrier height, δ_{sc}, has been known to be quite insensitive to the background cosmology as mentioned in Section 3.1. For the case of flat ΛCDM models, Eke et al. (1996) showed that δ_{sc} changes very mildly from 1.686 to 1.67 as Ω_m changes from 1 to 0.1. Even for the case of flat wCDM models, the weak dependence of δ_{sc} was rigorously proven by Pace et al. (2010) who directly solved the nonlinear differential equation of the density contrast in the spherical collapse process to find that the value of $\delta_{sc}(z)$ for the wCDM models remain very similar to that for the ΛCDM model in the whole redshift range.

Regarding the cosmology dependence of $\sigma(M, z)$, it depends on the background cosmology only through $D(z)$ and $P(k)$. Whereas, as can be seen in Figure 3.5, $\beta(z)$ differs even among those models which have the same shapes of $D(z)$ and $P(k)$. Therefore, the cosmology dependence of $\beta(z)$ witnessed in Figure 3.5 should come mainly from another channel, which we believe is the departure of δ_c from δ_{sc}. In different cosmologies, the non-spherical collapse in the nonlinear regime would proceed differently, resulting in the cosmology dependence of the degree of the departure of δ_c from δ_{sc}, which is described by the single parameter, $\beta(z)$, for the case of the field cluster abundance.

Without having a physical model for the effect of the background cosmology on the departure of δ_c from δ_{sc} at the moment, we find the following fitting formula useful to quantitatively describe the ways in which $\beta(z)$ differs among the eleven cosmologies and to efficiently assess the statistical significances of their differences:

$$\beta(z) = \beta_A \sinh^{-1}\left[\frac{1}{q_z}(z - z_c)\right], \tag{3.1}$$

where three adjustable parameters, β_A, q_z and z_c, denote the amplitude, redshift dispersion and critical redshift of $\beta(z)$, respectively. The overall amplitude, β_A, quantifies how much δ_c departs from the EdS value of δ_{sc} at $z = 0$, the critical redshift parameter, z_c, quantifies when δ_c becomes equal to δ_{sc}, while the inverse of the redshift dispersion,

$1/q_z$, quantifies the rate at which δ_c converges to δ_{sc}, as z increases. The best-fit values of (β_A, q_z, z_c) and their associated errors $(\sigma_{\beta_A}, \sigma_{q_z}, \sigma_{z_c})$ are obtained by fitting Equation (3.1) to the empirically determined $\beta(z)$ in Section 3.1 with the help of the non-linear least square code of SciPy python library by Virtanent et al. (2020) (see Table 3.2).

Figure 3.6 shows how well Equation (3.1) with three best-fit parameters (red solid line) describes the empirically determined $\beta(z)$ (filled circles), comparing the best-fit $\beta(z)$ for each of the ten wCDM cosmologies with that for the ΛCDM case (dashed line). It is interesting to see that the three cosmologies, ΛCDM, M007, and M009, which produce almost identical mass functions of the field clusters at all redshifts (Figures 3.2-3.4), can still be distinguished by their distinct $\beta(z)$. The differences in the best-fit values of the critical redshifts, Δ_{zc}, between the ΛCDM and M007 (M009) cases is as high as $3.47\sigma_{\Delta_{zc}}$ ($5.89\sigma_{\Delta_{zc}}$). Here, the errors, $\sigma_{\Delta_{zc}}$ is calculated through the error propagation as $\sigma_{\Delta_{zc}} \equiv \left(\sigma^2_{zc,1} + \sigma^2_{zc,2}\right)^{1/2}$ where $\sigma_{zc,1}$ and $\sigma_{zc,2}$ are the errors in the measurements of z_c for the ΛCDM and M007 (M009) cases, respectively. Note also that $\beta(z)$ can also distinguish between the two cosmologies, M002 and ΛCDM, although both of the cosmologies yield quite similar linear growth factors and field cluster mass functions (Figure 3.1). The difference, Δ_{zc}, between the two cosmologies is found to be as significant as $14\sigma_{\Delta_{zc}}$.

The evolution of $\beta(z)$ also allows us to distinguish not only between the wCDM and ΛCDM cosmologies but also among different wCDM cosmologies themselves. For instance, the two wCDM cosmologies, M001 and M006, are found to have almost no difference in their field cluster mass functions. Nevertheless, they can be distinguished by the $6.7\sigma_{\Delta_{zc}}$ differences in the best-fit values of z_c. These results clearly indicates a potential of $\beta(z)$ to complement the cluster mass function in discriminating the candidate cosmologies.

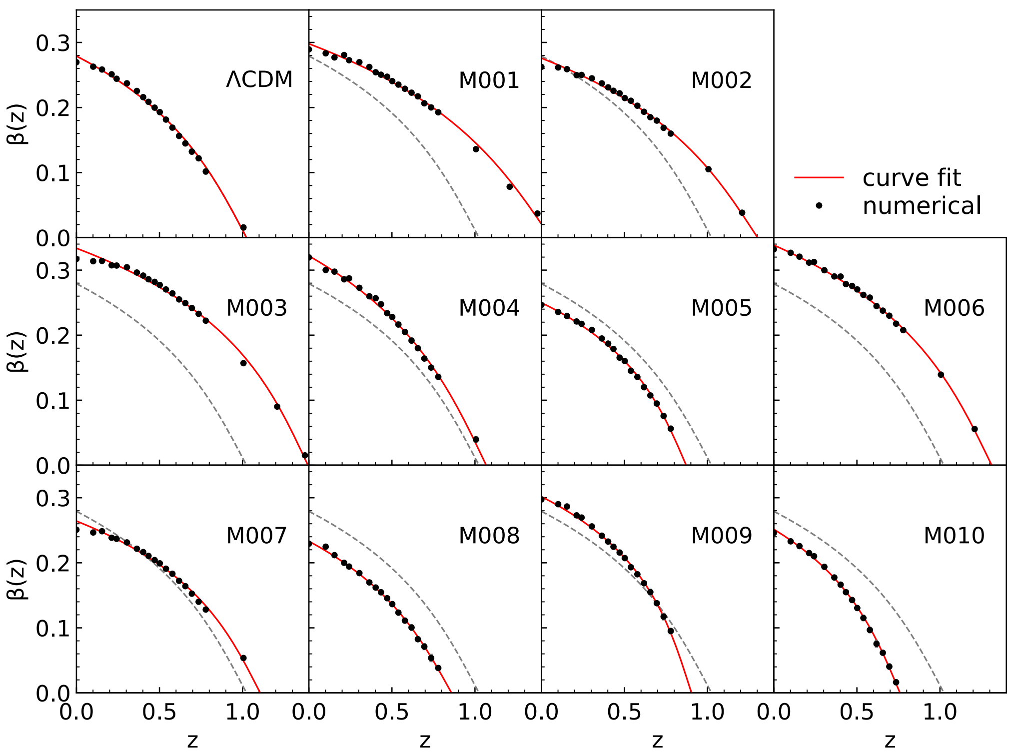

Figure 3.6. Linear fits (red solid lines) to the numerically obtained $\beta(z)$ (filled circles) for 11 different DE cosmologies.

Table 3.2. Best-fit parameters for the evolution of the drifting coefficient.

Cosmology	β_A	q_z	z_c
ΛCDM	-0.141 ± 0.008	0.289 ± 0.033	1.024 ± 0.014
M001	-0.147 ± 0.008	0.388 ± 0.045	1.456 ± 0.018
M002	-0.135 ± 0.005	0.343 ± 0.026	1.302 ± 0.014
M003	-0.138 ± 0.006	0.252 ± 0.026	1.394 ± 0.011
M004	-0.163 ± 0.008	0.303 ± 0.032	1.068 ± 0.014
M005	-0.111 ± 0.005	0.186 ± 0.018	0.872 ± 0.009
M006	-0.152 ± 0.005	0.285 ± 0.021	1.311 ± 0.012
M007	-0.116 ± 0.007	0.229 ± 0.031	1.106 ± 0.019
M008	-0.124 ± 0.005	0.269 ± 0.021	0.859 ± 0.007
M009	-0.120 ± 0.006	0.147 ± 0.019	0.903 ± 0.015
M010	-0.123 ± 0.004	0.199 ± 0.013	0.759 ± 0.005

Chapter 4

Probing Cosmology with the Isolated Cluster Mass Function

4.1 The Effect of Massive Neutrinos on $\beta(z)$

[1] We make an extensive use of the publicly available data from the Cosmological Massive Neutrinos Simulations (`MassiveNuS`) run by Liu et al. (2018) on a periodic box of comoving volume $512^3\,h^{-3}\,\mathrm{Mpc}^3$, containing 1024^3 particles, each of which is as massive as $10^{10}\,h^{-1}\,M_{\odot}$. The `MassiveNuS` was recurringly performed for one ΛCDM cosmology with massless neutrinos and for 100 different $\nu\Lambda$CDM cosmologies with massive neutrinos, whose initial conditions were described by the six key cosmological parameters as well as M_ν. For the study of the *sole* effect of the massive neutrinos on $dN_{\mathrm{I}}/d\ln M$ and $\beta(z)$, we consider only those cosmologies which have identical initial conditions other than M_ν with one another. Among the 101 cosmologies are found only 3 to meet this selection criterion, which have the same matter density parameter, $\Omega_m = 0.3$, and same amplitude of the primordial density power spectrum, $A_s = 2.1 \times 10^9$, but different total

[1] This section was published in Ryu, S. & Lee, J. 2020, ApJ, 894, 65.

neutrino mass, $M_\nu = 0.0,\ 0.1$ and 0.6 eV, respectively.

The `MassiveNuS` engaged the Rockstar algorithm (Behroozi et al. 2013) to find the DM halos at various redshifts and recorded such key properties of each Rockstar halo as its virial mass (M), virial radius, comoving position vector, peculiar velocity vector and so forth. From the catalog of the Rockstar halos resolved at each redshift for each of the three cosmologies, we numerically determine $dN_I/d\ln M$ and the analytical single parameter model, Equation (2.19), is fitted by adjusting the value of β following the same procedure arranged in Section 3.1 but with a linkage length parameter of $b_{\rm sc} = 0.33$ for the identification of the superclusters.

In the procedure of evaluating the analytic mass functions of the field clusters, the CAMB code (Lewis et al. 2000) is again exclusively used for $P(k, z)$. Note that since the linear growth factor, $D(z)$, acquires a scale dependence in the presence of massive neutrinos, the rms density fluctuation $\sigma(M, z)$, is no longer equal to $D(z)\sigma(M, z = 0)$. Instead, we calculate it as $\sigma(M, z) = \left[(2\pi^2)^{-1} \int dk\, k^2 P(k, z) W^2_{\rm th}(k, M)\right]^{1/2}$ where $W_{\rm th}$ is the spherical top-hat filter on the mass scale of M.

Figure 4.1 plots the linear density power spectra, $P(k, z)$, for the three different cases of M_ν at three different redshifts, computed by the CAMB code. As expected, the more massive neutrinos suppress more severely the linear density powers on the small scales ($k > 0.02\, h\,{\rm Mpc}^{-1}$). Note the small differences in $P(k, z)$ between the cases of $M_\nu = 0.0$ eV and $M_\nu = 0.1$ eV at all of the three redshifts. Given that the large uncertainties in the high-mass tails of the cluster mass functions caused by poor-number statistics and cosmic variance are likely to exceed this small differences in $P(k, z)$, the cluster mass functions would be unable to discriminate the two $\nu\Lambda$CDM cosmologies from each other.

Figure 4.2 displays both of the numerical field cluster mass functions from the `MassiveNuS` (filled circles) and the analytic model with the best-fit value of β (red

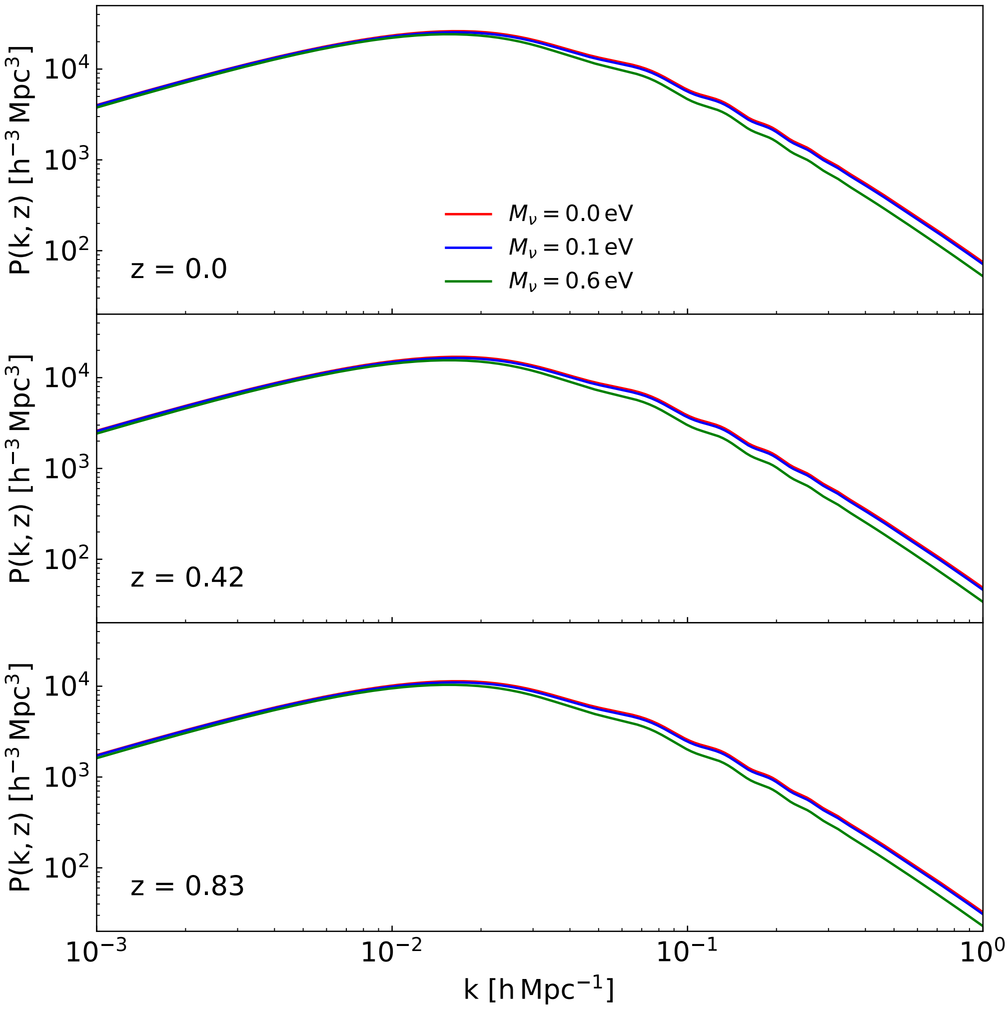

Figure 4.1. Linear density power spectra for three different values of total neutrino mass ($M_\nu = 0.0,\ 0.1,\ 0.6$ eV) at three different redshifts ($z = 0.0,\ 0.42,\ 0.83$), computed by the CAMB code (Lewis et al. 2000).

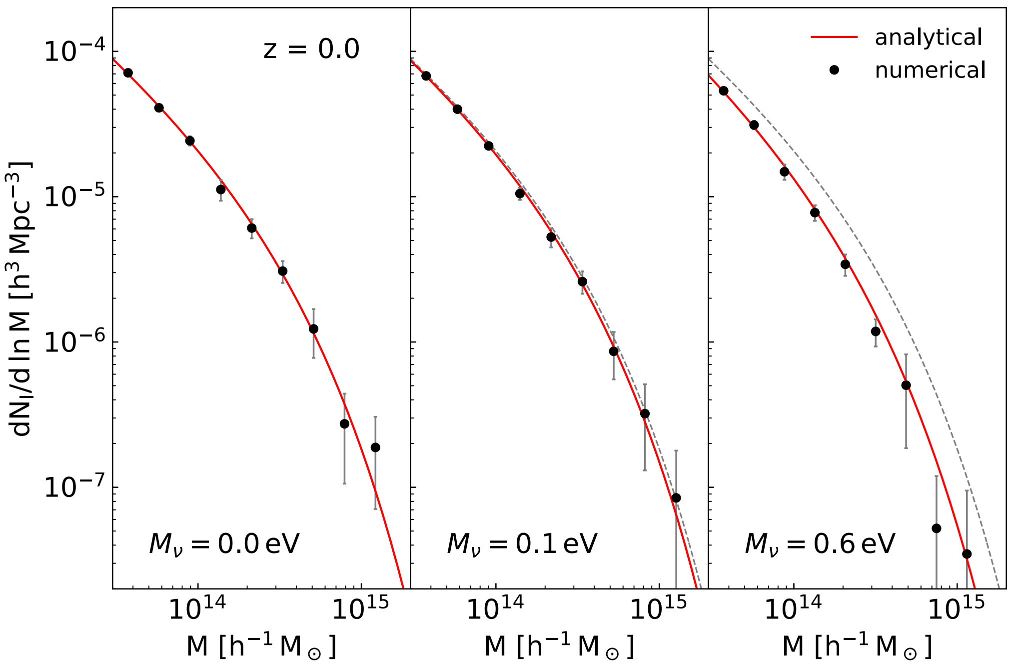

Figure 4.2. Analytic mass functions of the field clusters (red solid lines) over-plotted with the numerical results from the `MassiveNuS` for the three different cases of M_ν at $z = 0$. The dashed lines in the middle and right panels conform to the red solid line in the left panel.

solid lines) at $z = 0$ for the three different cases of M_ν. The grey dashed lines in the middle and right panels conform to the red solid line in the left panel. Figures 4.3-4.4 show the same as Figure 4.2 but at $z = 0.42$ and 0.83, respectively. As can be seen, the analytical single parameter model for $dN_{\rm I}/d\ln M$ agrees excellently well with the numerical results at all redshifts for all of the three cases of M_ν, confirming its validity even in the presence of massive neutrinos and proving its robustness as a physical model.

Figures 4.2-4.4 clearly show that $dN_{\rm I}/d\ln M$ has a significantly lower amplitude for the case of $M_\nu = 0.6\,{\rm eV}$ than for the other two cases of $M_\nu = 0.0\,{\rm eV}$ and $M_\nu = 0.1\,{\rm eV}$,

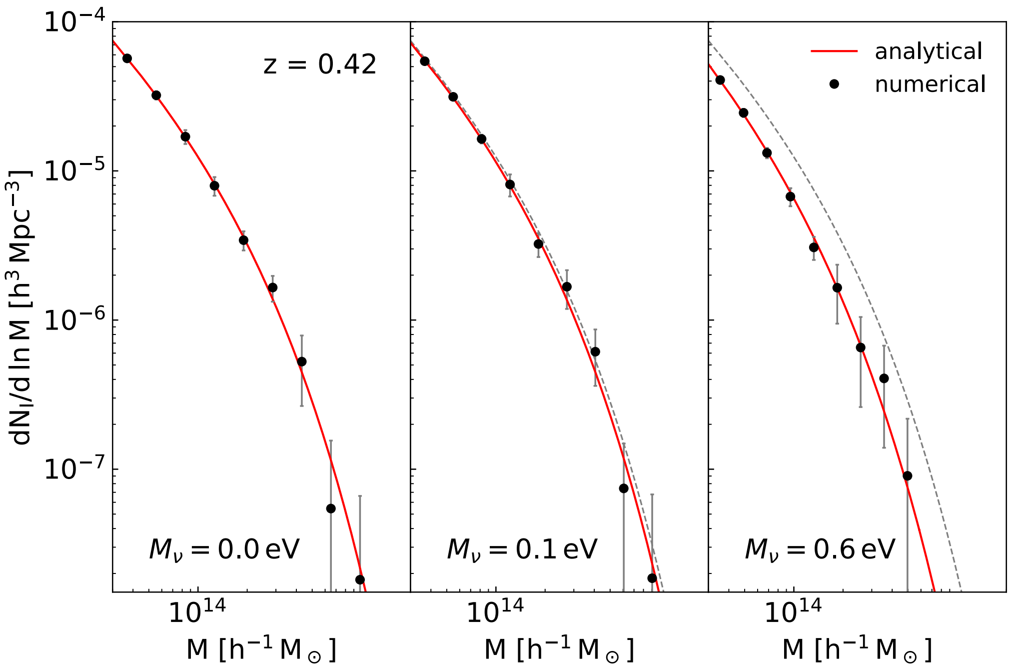

Figure 4.3. Same as Figure 4.2 but for at $z = 0.42$.

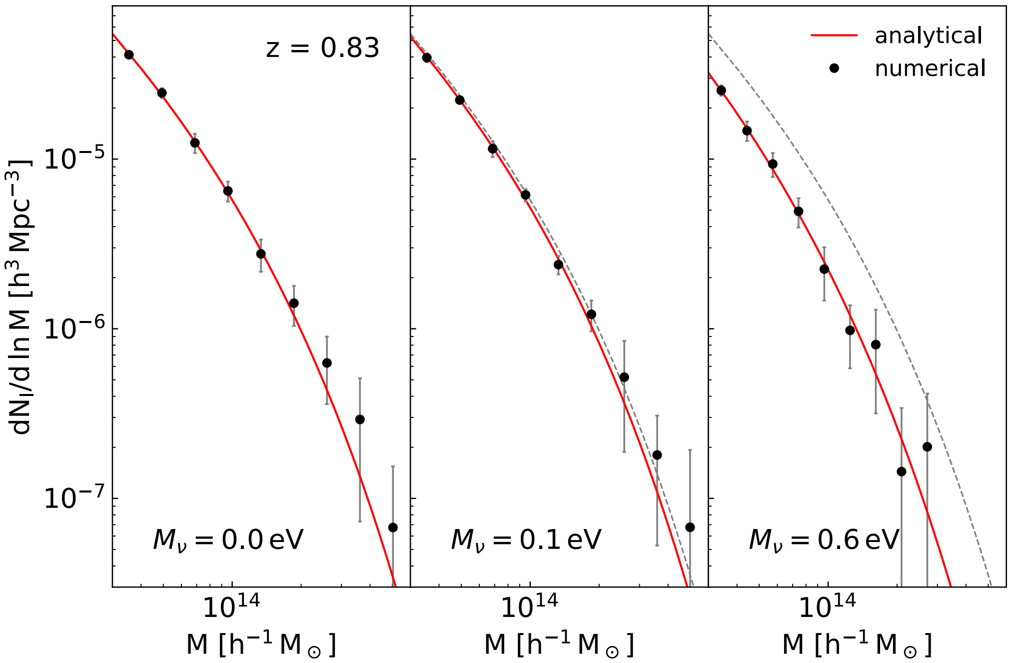

Figure 4.4. Same as Figure 4.2 but for at $z = 0.83$.

between which almost no difference is found in $dN_{\rm I}/d\ln M$, no matter at what redshifts they are compared with each other. Although the difference in $dN/d\ln M$ between the two cases of $M_\nu = 0.0\,\mathrm{eV}$ and $M_\nu = 0.1\,\mathrm{eV}$ tends to slightly increase with z, the larger errors in the measurement of $dN_{\rm I}/d\ln M$ at higher redshifts weigh down their statistical significances. The comparison of Figures 4.2-4.4 with Figure 4.1 indicates that the M_ν-dependence of the field cluster mass function is almost entirely dictated by the M_ν-dependence of $P(k, z)$. As mentioned in Section 2, the cosmology-dependence of the field cluster abundance (including its M_ν-dependence) has two different sources, $P(k, z)$ and β. The results shown in Figures 4.2-4.4, however, imply that the former overwhelms the latter in shaping the M_ν-dependence of the field cluster mass function, which in turn warns that the field cluster mass function would fail not only in constraining M_ν below the Planck constraint but also in breaking the σ_8-M_ν degeneracy.

Figure 4.5 plots the numerically determined values of $\beta(z)$ at twenty different redshifts in the range of $0 \le z \le 1$ for the three different cases of M_ν, revealing that $\beta(z)$ evolves differently among the three cases. As can be seen, at $z \lesssim 0.3$ the drifting coefficient $\beta(z)$ has higher values for the case of $M_\nu = 0.6\,\mathrm{eV}$ than for the other two cases. Whereas at $z \gtrsim 0.3$, the tendency is reversed. The most massive neutrinos case yields the lowest values of $\beta(z)$, while its highest values are found for the massless neutrinos case. In addition, we find that the slope of $\beta(z)$ substantially differs even between the two cases of $M_\nu = 0.0\,\mathrm{eV}$ and $M_\nu = 0.1\,\mathrm{eV}$, while no difference found in $\beta(z = 0)$ between them.

We speculate that this redshift-dependence of the effect of massive neutrinos on $\beta(z)$ might help break the σ_8-M_ν degeneracy. Recall that the effect of massive neutrinos on the linear density power spectra and cluster mass function is consistent in its direction, regardless of the redshifts, as witnessed in Figures 4.1-4.4. The more massive neutrinos always reduce more severely the amplitudes of $P(k, z)$ and $dN_{\rm I}/d\ln M$ at all redshifts,

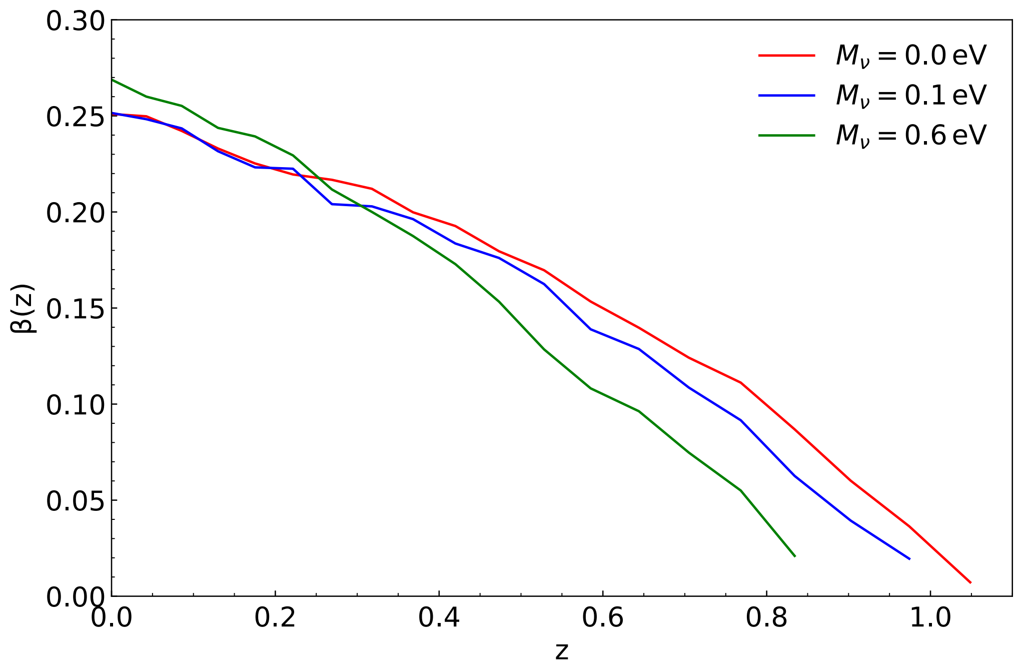

Figure 4.5. Numerical results of the drifting coefficient, $\beta(z)$, in the redshift range of $0 \leq z \leq 1$ for the three different cases of M_ν, from the `MassiveNuS`.

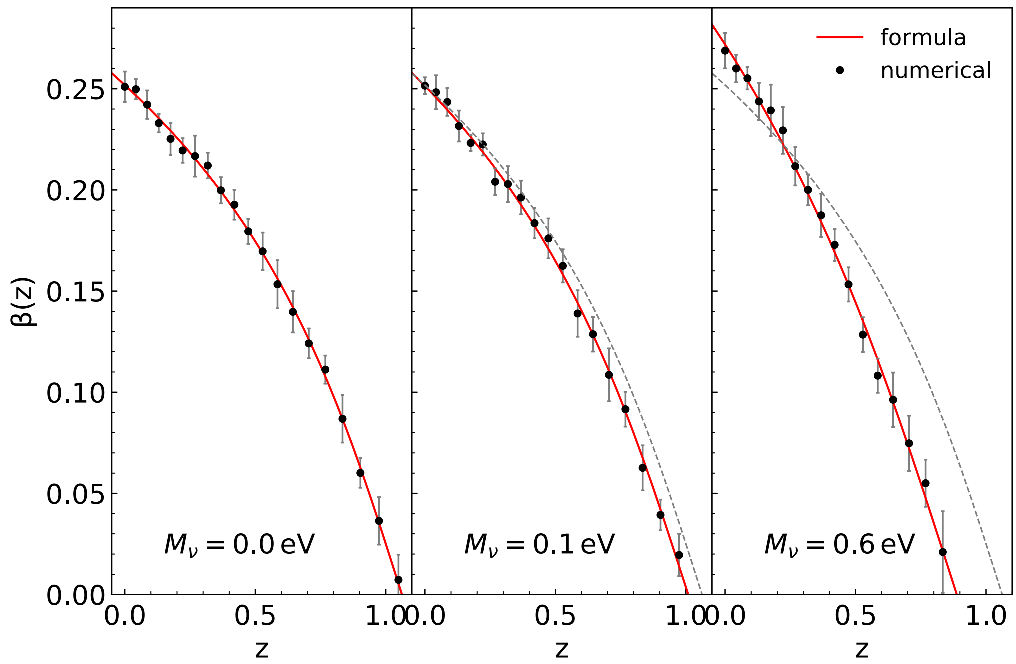

Figure 4.6. Best-fit formula for $\beta(z)$ (red solid line) over-plotted with the numerical results (filled circles) for the three different cases of M_ν. The dashed lines in the middle and right panels conform to the red solid line in the left panel.

which is why the two diagnostics suffer from the σ_8-M_ν degeneracy. In other words, the lower value of σ_8 has the same effect on $P(k, z)$ (and $dN/d\ln M$ as well) as the higher value of M_ν. Meanwhile, our result shown in Figure 4.5 implies that the effect of the higher value of M_ν on $\beta(z)$ might be differentiated from that of the lower value of σ_8 on $\beta(z)$. The latter lowers the amplitude of $\beta(z)$ without changing its slope, while the former heightens its amplitude and concurrently steepens its slope. Yet, the possibility of breaking the σ_8-Ω_m degeneracy with $\beta(z)$ is only a speculation, since we have yet to demonstrate its feasibility in practice.

As done in Section 3.2, to effectively quantify the differences in the evolution of the drifting coefficient among the three cosmologies, we fit Equation (3.1) to the numerically

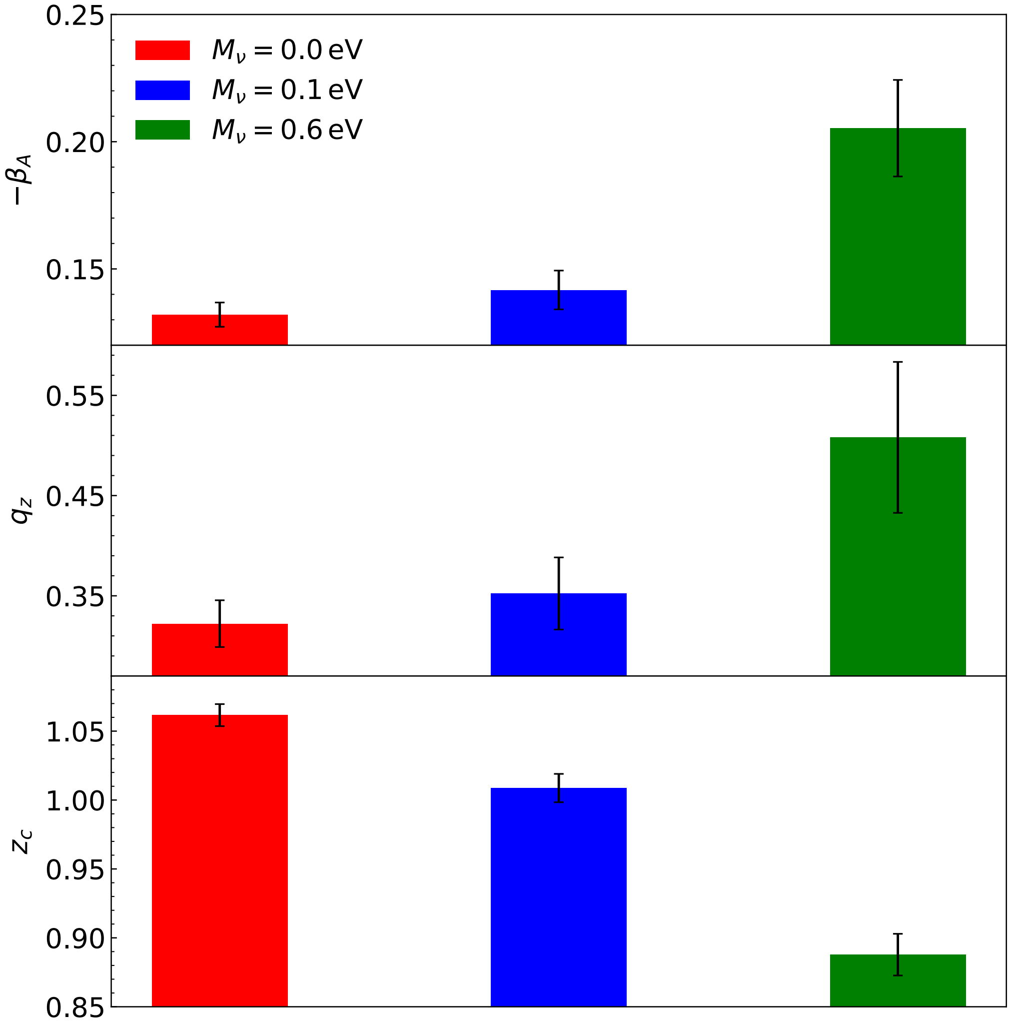

Figure 4.7. Best-fit three parameters of the analytic formula for $\beta(z)$ for the three different cases of M_ν.

determined $\beta(z)$ by adjusting the values of β_A, q_z and z_c to yield the minimum χ^2. Figure 4.6 demonstrates how well the simple formula (red solid lines), Equation (3.1), agrees with the numerically obtained $\beta(z)$ (black filled circles) for all of the three cases of M_ν. Figure 4.7 shows the best-fit values of $-\beta_A$, q_z, z_c with their errors σ_{β_A}, σ_{qz}, σ_{zc}, which are all obtained through the χ^2 fitting after due consideration of the uncertainties in $\beta(z)$ shown in Figure 4.6.

The most significant differences among the three cases are found in the values of z_c, which is consistent with the result of Section 3.2, that z_c was found to vary most sensitively with the dark energy equation of state. Assessing the statistical significances of the differences in z_c among the three cases of M_ν by estimating the errors of their mutual differences, $\sigma_{\Delta(zc)}$, propagated from σ_{zc}, as done in Section 3.2, we find the difference in z_c between the two cases of $M_\nu = 0.0\,\mathrm{eV}$ and $M_\nu = 0.1\,\mathrm{eV}$ ($M_\nu = 0.6\,\mathrm{eV}$) to exceed $4\sigma_{\Delta(zc)}$ ($10\sigma_{\Delta(zc)}$). Whereas, the differences in the other two parameters, β_A and q_z, between the two cases of $M_\nu = 0.0\,\mathrm{eV}$ and $M_\nu = 0.1\,\mathrm{eV}$ ($M_\nu = 0.6\,\mathrm{eV}$) are found to be statistically insignificant (not so significant as that in z_c).

It should be worth explaining here why z_c is the most sensitive to the variation of M_ν. Given the definition z_c as a critical redshift at which $\delta_c = 1.686$ (i.e, $\beta(z_c) = 0$), its value should be determined by two factors, both of which sensitively depend on M_ν. The first factor is how fast the matter density parameter Ω_m approaches unity (i.e, the Einstein-de Sitter value) at high redshifts, while the second one is how rare the field clusters are in a given universe, since the gravitational collapse of the rarer objects proceeds in a more spherically symmetrical way (Bernardeau 1994). Meanwhile, the other two parameters, β_A and q_z, depend mainly on either of the two factors: β_A on the second, while q_z on the first.

4.2 Effect of Coupled Dark Energy on $\beta(z)$

[2] A cDE cosmology describes an alternative universe where the role of DE is played by a dynamical scalar field, ϕ, coupled to DM particles through energy-momentum exchange. The DE-DM coupling that causes the time-variation of DM particle mass (Wetterich 1995; Amendola 2000, 2004) generates a long-range fifth force via which the growth of structures can be enhanced (e.g., Mangano et al. 2003; Macciò et al. 2004; Mainini & Bonometto 2006; Pettorino & Baccigalupi 2008; Baldi et al. 2010; Wintergerst & Pettorino 2010, and references therein). Categorized by the shape of DE self-interaction potential, $V(\phi)$, as well as by the strength of the DE-DM coupling, $s(\phi) \equiv -d \ln m_{\rm DM}/d\phi$, a cDE cosmology has recently attained delving attentions since it has been found to provide a possible solution to the Hubble tension (Di Valentino et al. 2020).

To investigate the effect of cDE on the redshift evolution of $\beta(z)$, we utilize the data from the Large Coupled Dark Energy Cosmological Simulations (L-CoDECS) run by Baldi (2012a) with a modified version of the GADGET3 code, a non-public developers version of the widely-used public code GADGET-2 (Springel 2005). The L-CoDECS is a series of N-body cosmological runs that simulate a standard ΛCDM and five different cDE cosmologies on a periodic box of linear size $1\,h^{-1}$Gpc containing 1024^3 collisionless DM particles of individual mass $m_{\rm DM} = 5.84 \times 10^{10}\,h^{-1}M_{\odot}$ as well as an equal number of collisionless baryon particles of $m_{\rm baryon} = 1.17 \times 10^{10}\,h^{-1}M_{\odot}$. The initial conditions of the standard ΛCDM cosmology were chosen to meet the constraints from the Seven-Year Wilkinson Microwave Anisotropy observations (Komatsu et al. 2011). The five different cDE cosmologies are divided into three categories: the constant DM-DE coupling and exponential potentials (EXP001, EXP002, EXP003), the

[2] This section was published in Ryu, S., Lee, J., & Baldi, M. 2020, ApJ, 904, 93.

Table 4.1. Best-fit Parameters of $\beta(z)$ for the CoDECS cosmologies.

Model	$V(\phi)$	s	σ_8	β_A	q_z	z_c
ΛCDM	-	-	0.809	-0.16 ± 0.01	0.31 ± 0.04	1.10 ± 0.02
EXP001	$e^{-0.08\phi}$	0.05	0.825	-0.16 ± 0.01	0.31 ± 0.05	1.04 ± 0.02
EXP002	$e^{-0.08\phi}$	0.10	0.875	-0.17 ± 0.02	0.35 ± 0.08	1.32 ± 0.04
EXP003	$e^{-0.08\phi}$	0.15	0.967	-0.14 ± 0.01	0.19 ± 0.06	1.44 ± 0.05
EXP008e3	$e^{-0.08\phi}$	0.40	0.895	-0.16 ± 0.01	0.27 ± 0.04	1.19 ± 0.03
SUGRA003	$\phi^{-2.15}e^{\phi^2/2}$	-0.15	0.806	-0.16 ± 0.01	0.39 ± 0.07	1.35 ± 0.03

exponential DM-DE coupling and exponential potential (EXP008e3) and the constant coupling and supergravity potential (SUGRA). All cDE cosmologies simulated by the L-CoDECS were ensured to have a flat geometry, sharing the same values of the five key cosmological parameters, $h = 0.703$, $\Omega_{\rm CDM} = 0.226$, $\Omega_{\rm DE} = 0.729$, $\Omega_b = 0.0451$, $A_s = 2.42 \times 10^{-9}$ and $n_s = 0.966$. They differ from one another only in the potential shape and DM-DE coupling as well as in the linear density power spectrum amplitude, information on which are provided in the first four columns of Table 4.1. For more detailed description of the cDE cosmologies and the L-CoDECS [3], we refer the readers to Baldi (2012a,b).

The L-CoDECS simulations have been released with catalogs of gravitationally bound halos identified for each cosmology through a two-step process starting with a Friends-of-Friends (FoF) algorithm with linking length parameter of $b_c = 0.2$ followed by a gravitational unbinding procedure of each individual FoF halo using the SUBFIND al-

[3]All data are available at the CoDECS website, http://www.marcobaldi.it/web/CoDECS.html

gorithm (Springel et al. 2001) that allows to associate spherical overdensity masses and radii to each gravitationally bound main substructure. Analyzing the FoF halo catalogs, the differential mass function of the field clusters halos, $dN_{\rm I}/d\ln M$, is determined as explained in Section 3.1. Using the linear density power spectrum of each cDE cosmology provided within the CoDECS public data release, we evaluate the linear density rms fluctuation, $\sigma(M)$, and the analytic mass function of the field cluster, Equation (2.19), as well. The best-fit value of the drifting coefficient, β in Equation (2.19) is determined at each redshift (Section 3.1). As done in Section 3.1, once the values of $\beta(z)$ are determined at various redshifts, we fit them to Equation (3.1) to find the best-fit values of the three parameters, β_A, q_z and z_c and their associated errors σ_{β_A}, σ_{q_z} and σ_{z_c}, respectively (see Table 4.1). Then, we calculate the statistical significance of the differences in the three parameters among the cosmologies as $\Delta\beta_A/\sigma_{\Delta\beta_A}$, $\Delta q_z/\sigma_{\Delta q_z}$ and $\Delta z_c/\sigma_{\Delta z_c}$ where $\Delta\beta_A$, Δq_z and Δz_c are the differences in the three parameters between two cosmologies, while $\sigma_{\Delta\beta_A}$, $\sigma_{\Delta q_z}$ and $\sigma_{\Delta z_c}$ correspond to the propagated errors in the determination of the differences.

Figure 4.8 (Figure 4.9) plots the numerically determined mass functions of the field cluster halos (filled black circles) as well as the analytic model (red solid line), Equation (2.19), with the best-fit value of β for the six cosmologies at $z=0$ ($z=1$), respectively. In each panel, the analytic model for the ΛCDM case (grey dashed line) is also plotted to show the differences. Although the analytic model, Equation (2.19), succeeds in matching the numerical results at both of the redshifts for all of the cDE cosmologies, the field cluster mass functions are found to be incapable of telling apart with high statistical significance the three cosmologies ΛCDM, EXP001 and SUGRA at both of the redshifts, $z=0$ and 1.

Figure 4.10 plots the redshift evolution of the empirically determined drifting coefficient, $\beta(z)$ (filled black circles) as well as the fitting formula (red solid lines) for the six

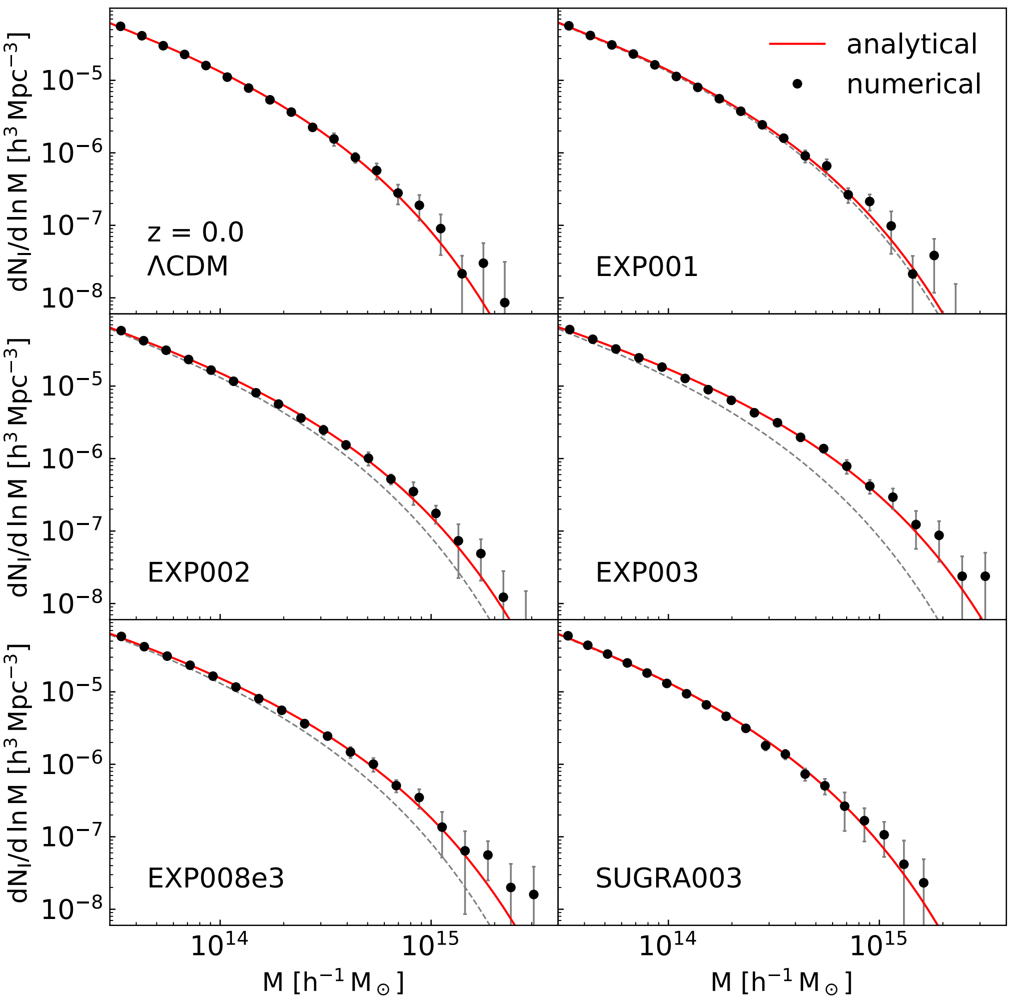

Figure 4.8. Field cluster mass functions numerically obtained (black filled circles) from the CoDECS and analytic model with the best-fit drifting coefficient (red solid lines) for a ΛCDM and five different cDE cosmologies at $z = 0$.

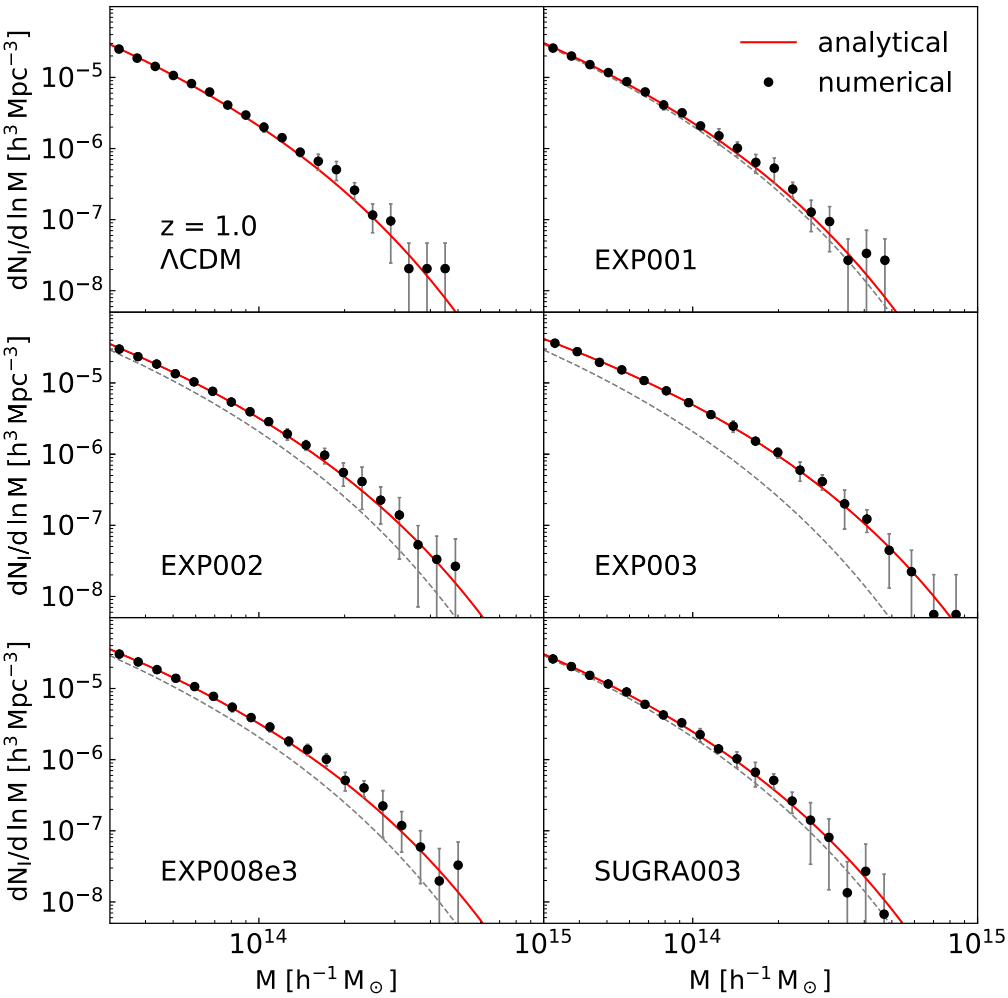

Figure 4.9. Same as Figure 4.8 but at $z = 1$.

cosmologies. In each panel, the fitting formula for the ΛCDM case (grey dashed line) are also plotted to show the differences. As can be seen, the fitting formula expressed in terms of the inverse sine hyperbolic function, Equation (3.1), with the best-fit values of q_z, β_A and z_c indeed describes quite well the behaviors $\beta(z)$ for all of the six cosmologies. Note that the SUGRA can be distinguished by $\beta(z)$ from the ΛCDM with high statistical significance despite that the two cosmologies are mutually degenerate in the cluster mass functions. The statistical significance of the difference in the critical redshift parameter, z_c, between the ΛCDM and the SUGRA cosmologies is found to be as high as $7.48\,\sigma$. Although $\beta(z)$ distinguishes with high statistical significance the other cDE cosmologies except for the EXP001 from the ΛCDM, it fails to break the degeneracy between the ΛCDM and the EXP001 cases, due to the extremely weak DM-DE coupling of the latter cosmology.

We have so far used prior information on the background cosmology for the determination of $dN_{\rm I}/d\ln M$ and $\beta(z)$. In other words, to examine if $\beta(z)$ can break a cosmic degeneracy between two different cosmologies, we assume that information on the shape of the linear density power spectrum are available. In practice, however, this prior information is not available for the determination of $\beta(z)$. Especially, if a background cosmology is indistinguishable from the ΛCDM case by the standard diagnostics, then it may not be justified to make such a preemptive assumption about the shape of the linear density power spectrum. The EXP001 corresponds to this case where no prior information on the background cosmology should be assumed to be available in practice, since the standard diagnostics including the linear density power spectrum, mass function, etc., are unable to distinguish it from the ΛCDM case.

To deal with this degeneracy, we use the linear density power spectrum of the ΛCDM case, $P(k;\Lambda\mathrm{CDM})$, for the computation of $\sigma(M)$ in $dN_{\rm I}/d\ln M$ for the EXP001 case and compare the reevaluated analytic model with the numerical results to find the

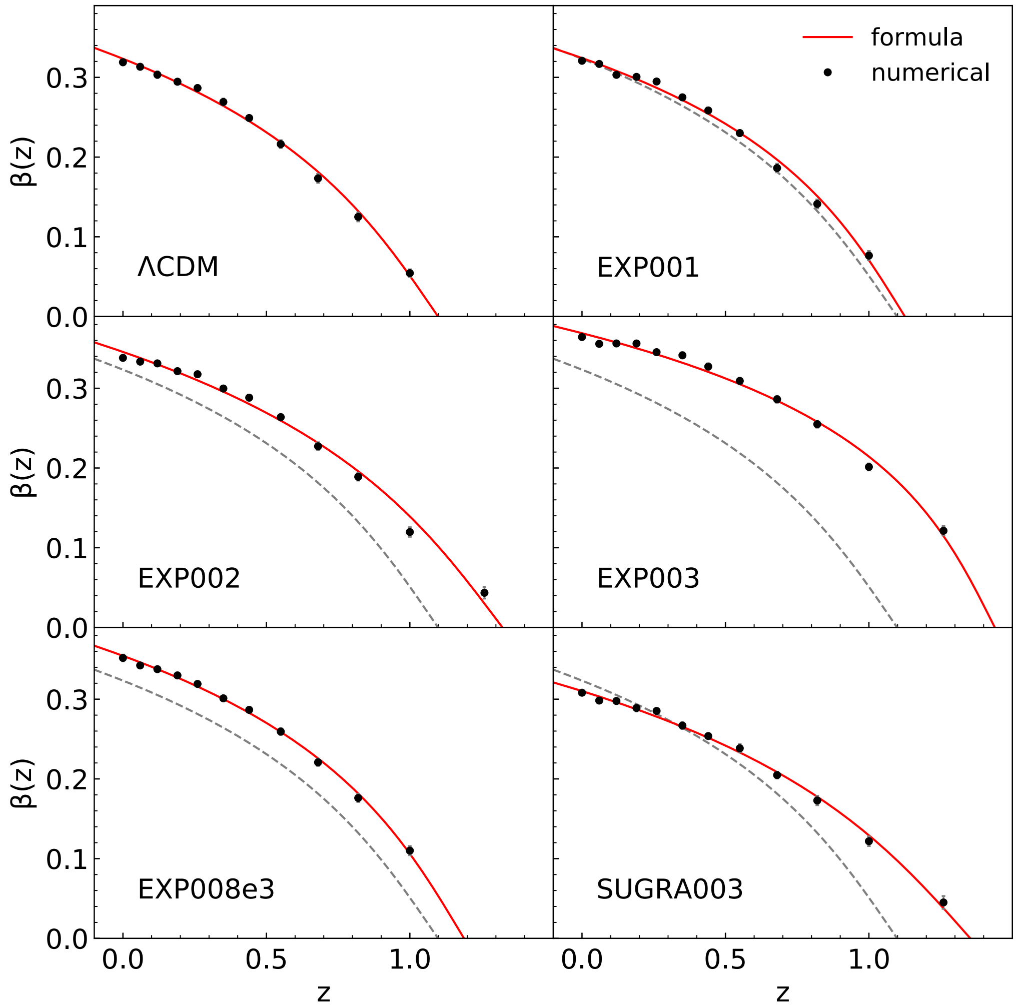

Figure 4.10. Empirically determined redshift evolution of the drifting coefficient of the field clusters (black filled circles) and fitting formula (red solid lines) for ΛCDM and five different cDE cosmologies.

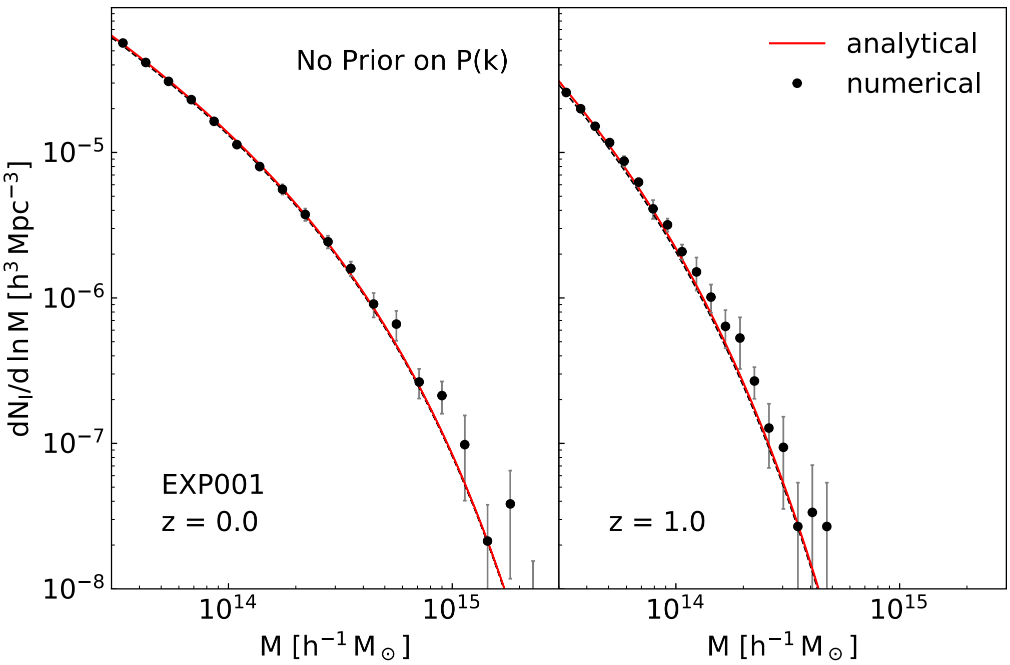

Figure 4.11. Field cluster mass functions for the EXP001 case determined without using prior information on $P(k)$.

best-fit $\beta(z)$. That is, we redetermine $\beta(z)$ for the EXP001 case without using prior information on $P(k;\mathrm{EXP001})$. Figure 4.11 plots the analytical mass function of the field clusters (red solid lines) obtained by using $P(k;\Lambda\mathrm{CDM})$ and compares it with the numerical results (black filled circles) for the EXP001 case at $z = 0$ (top panel) and $z = 1$ (bottom panel). As can be seen, in spite of no prior information on the background cosmology, the analytical mass function of the field clusters still describes quite well the numerical results at both of the redshifts for the EXP001 case.

Figure 4.12 plots the same as the top-right panel of Figure 4.10 but without using prior information on $P(k;\mathrm{EXP001})$. As can be seen, the EXP001 turns out to yield larger differences in $\beta(z)$ from the ΛCDM. The best-fit values of β_A, q_z and z_c for the EXP001 case listed in Table 4.1 correspond to the ones obtained without using prior in-

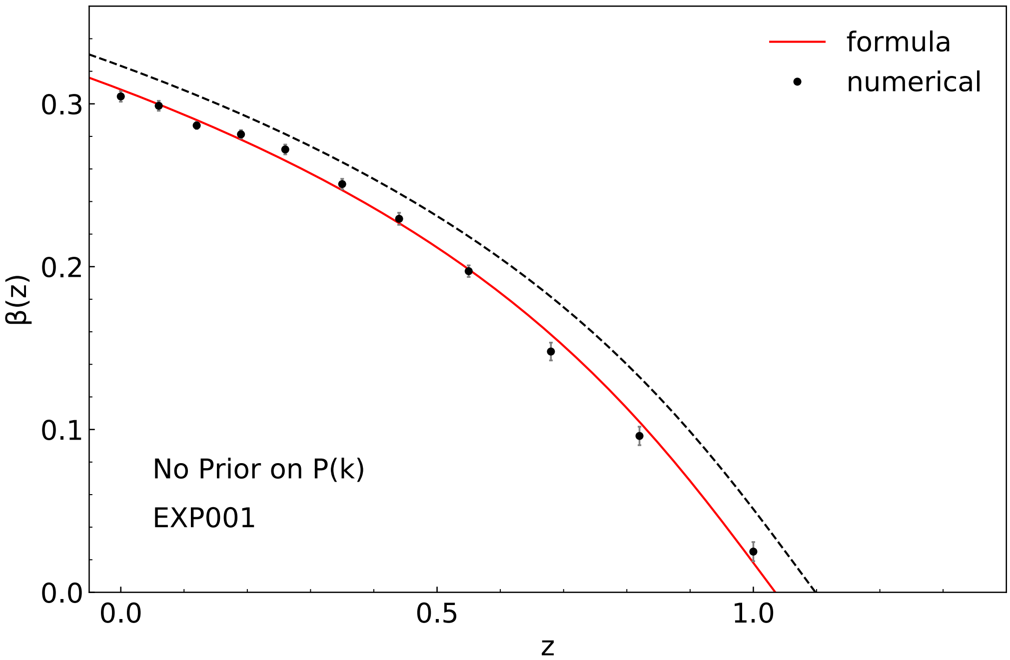

Figure 4.12. Evolution of the drifting coefficient of the field clusters for the EXP001 case determined without using prior information on $P(k)$

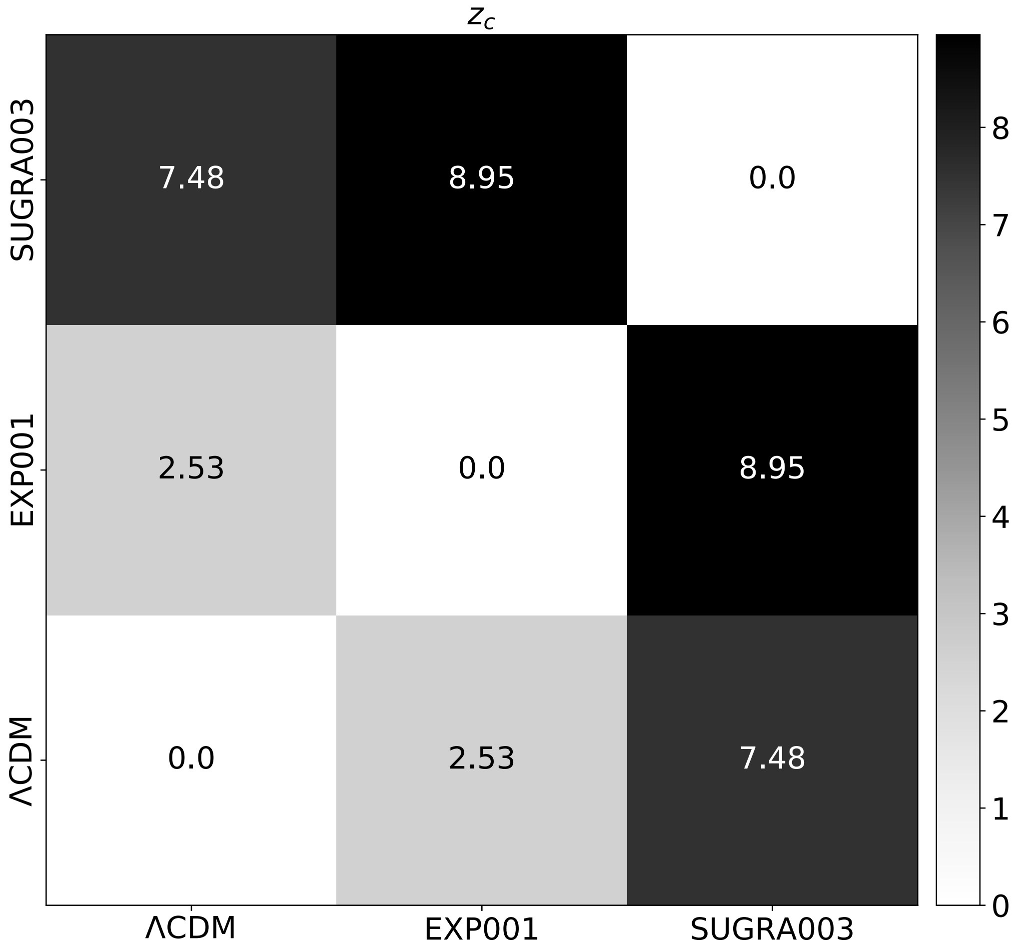

Figure 4.13. Statistical significances of the differences among the ΛCDM, EXP001, and SUGRA that are mutually degenerate in the cluster mass functions.

formation on $P(k; \mathrm{EXP001})$. The statistical significance of the difference in z_c between the ΛCDM and the EXP001 is found to be as high as 2.53. Figure 4.13 summarizes the statistical significance of the difference in z_c among the three cosmologies, ΛCDM, EXP001, and SUGRA, which are mutually degenerate in the field cluster mass functions. Although the degeneracy between the ΛCDM and the EXP001 can be broken by $\beta(z)$ only with 2.53 significance, we speculate that a larger data set would improve the significance.

4.3 Effect of $f(R)$ Gravity on $\beta(z)$

[4] In the theory of $f(R)$ gravity, the strength of a long range fifth force is quantified by the absolute value of the derivative of $f(R)$ with respect to the Ricci scalar R at the present epoch, $|f_{R0}| \equiv |df/dR|_0$. A larger value of $|f_{R0}|$ corresponds to a stronger fifth force, which would more severely enhance the small-scale density power (Hu & Sawicki 2007; Li & Barrow 2007). If neutrinos have a non-zero mass in a $f(R)$ gravity cosmology, however, the suppressing effect of the free streaming neutrinos on the small-scale density power spectrum could compensate the enhancing effect of the fifth force, resulting in a suppression of the deviations from the standard ΛCDM + GR cosmology that each of these two scenarios would individually imprint on structure formation. In other words, the linear density power spectra may not be capable of distinguishing a certain combination of f_{R0} with $\sum m_\nu$ from the standard ΛCDM + GR cosmology, since they could have zero net effect on the amplitude of small-scale density perturbations (e.g., Baldi et al. 2014).

To investigate if $\beta(z)$ can also break the cosmic degeneracy between ΛCDM+GR and νCDM+$f(R)$, we use a subset of the data from the DUSTGRAIN-*pathfinder* N-

[4]This section was published in Ryu, S., Lee, J., & Baldi, M. 2020, ApJ, 904, 93.

body simulation suite that were conducted by Giocoli et al. (2019) on a box of volume $750^3\,h^{-3}\mathrm{Mpc}^3$ for various νCDM+$f(R)$ cosmologies as well as the ΛCDM+GR cosmology. The DUSTGRAIN-*pathfinder* simulations were performed with the MG-GADGET code (Puchwein et al. 2013) – another modified version of GADGET-3 implementing an adaptive mesh solver for the spatial fluctuations of the f_R scalar degree of freedom – to trace the evolution of 768^3 DM particles of mass $8.1 \times 10^{10}\,h^{-1}M_\odot$. To simulate the νCDM+$f(R)$ cosmologies, the DUSTGRAIN-*pathfinder* adopted the widely-used realisation of $f(R)$ proposed by Hu & Sawicki (2007) and a particle-based implementation of massive neutrinos developed by Viel et al. (2010). Collapsed structures were identified through a FoF finder with a linking length parameter of $b_c = 0.16$ followed by the unbinding procedure implemented in the SUBFIND code to identify the halo center and its spherical overdensity mass and radius for all gravitationally bound objects in each cosmology, similarly to what described above for the CoDECS simulations. For a detailed description of the technical details of the DUSTGRAIN-*pathfinder* simulations, see Giocoli et al. (2019).

Among the various cosmologies simulated by the DUSTGRAIN-*pathfinder*, we consider three different CDM+$f(R)$ (namely, fR4, fR5 and fR6 corresponding to $|f_{R0}| = 10^{-4},\ 10^{-5}$ and 10^{-6}, respectively) and three different νCDM+$f(R)$ (namely fR4+0.3 eV, fR5+0.15 eV and fR6+0.06 eV corresponding to $\sum m_\nu = 0.3\,\mathrm{eV},\ 0.15$ and $0.06\,\mathrm{eV}$, respectively) as well as the standard ΛCDM + GR (from here on, GR) with initial conditions set at the Planck values (Planck Collaboration et al. 2016). These 7 different cosmologies were ensured to be flat, described by the common key cosmological parameter values of $h = 0.67$, $\Omega_m = 0.31$, $\Omega_{\mathrm{DE}} = 0.67$, $\Omega_b = 0.0481$, $A_s = 2.2 \times 10^{-9}$ and $n_s = 0.97$. The first four columns of Table 4.2 list the values of $|f_{R0}|$, $\sum m_\nu$, σ_8 for each of the seven cosmologies considered in the present work.

We first examine whether or not the analytic model for the field cluster mass func-

Table 4.2. Best-fit Parameters of $\beta(z)$ for the DUSTGRAIN-pathfinder cosmologies.

Model	$\|f_{R0}\|$	$\sum m_\nu$ [eV]	σ_8	β_A	q_z	z_c
ΛCDM	-	0.0	0.847	-0.11 ± 0.01	0.22 ± 0.06	1.24 ± 0.03
fR4	10^{-4}	0.0	0.967	-0.10 ± 0.01	0.16 ± 0.04	1.39 ± 0.03
fR5	10^{-5}	0.0	0.903	-0.16 ± 0.02	0.50 ± 0.11	1.40 ± 0.04
fR6	10^{-6}	0.0	0.861	-0.08 ± 0.01	0.09 ± 0.04	1.24 ± 0.04
fR4+0.3eV	10^{-4}	0.3	0.893	-0.09 ± 0.01	0.29 ± 0.09	1.52 ± 0.06
fR5+0.15eV	10^{-5}	0.15	0.864	-0.15 ± 0.05	0.85 ± 0.45	1.73 ± 0.14
fR6+0.06eV	10^{-6}	0.06	0.847	-0.08 ± 0.01	0.11 ± 0.04	1.27 ± 0.04

tion, Equation (2.19), is valid for the three CDM+$f(R)$ cosmologies. Analyzing the FoF halo catalogs in the redshift range $0 \le z \le 1$ and following the same procedure described in Section 3.1, we numerically determine $dN_{\rm I}/d\ln M$ for the GR, fR4, fR5 and fR6 cases. To evaluate the analytic model, Equation (2.19), and compare it with the numerically determined $dN_{\rm I}/d\ln M$ to derive $\beta(z)$ for each of the three $f(R)$ gravity cosmologies, we use the MGCAMB code (Zhao et al. 2009; Hojjati et al. 2011; Zucca et al. 2019; Lewis et al. 2000).

Figure 4.14 (Figure 4.15) depicts the numerical mass functions of the field cluster halos (filled black circles) as well as the analytic model (red solid line) and ΛCDM case comparison (grey dashed line) for the four cosmologies at $z = 0$ ($z = 1$), respectively, revealing that the analytic model matches quite well the numerical results even for the $f(R)$ gravity models. As expected, the fR4 (fR6) yields the most (least) abundant field clusters in the entire mass range. No statistically significant difference is found in

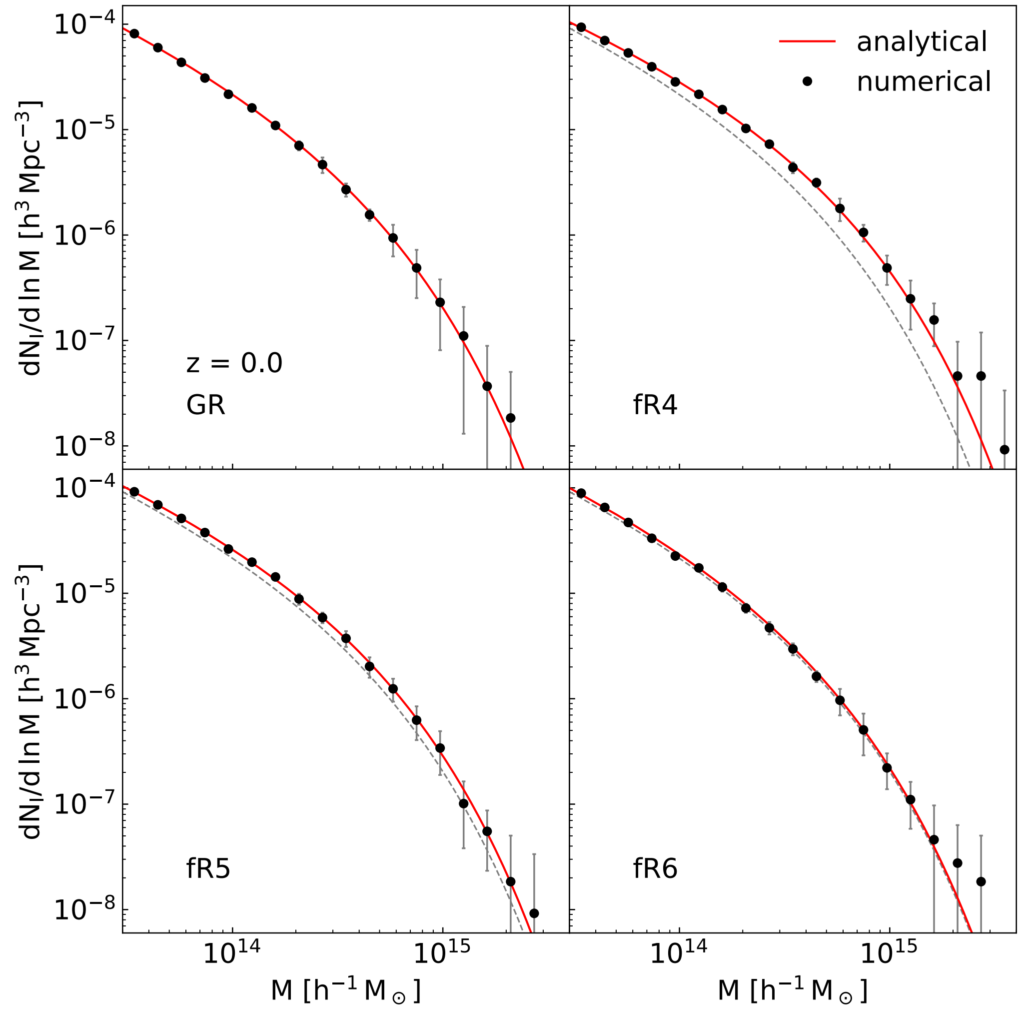

Figure 4.14. Field cluster mass functions numerically obtained (black filled circles) from the DUSTGRAIN-*pathfinder* and analytic model with the best-fit drifting coefficient (red solid lines) for a ΛCDM and three different $f(R)$ gravity cosmologies at $z = 0$.

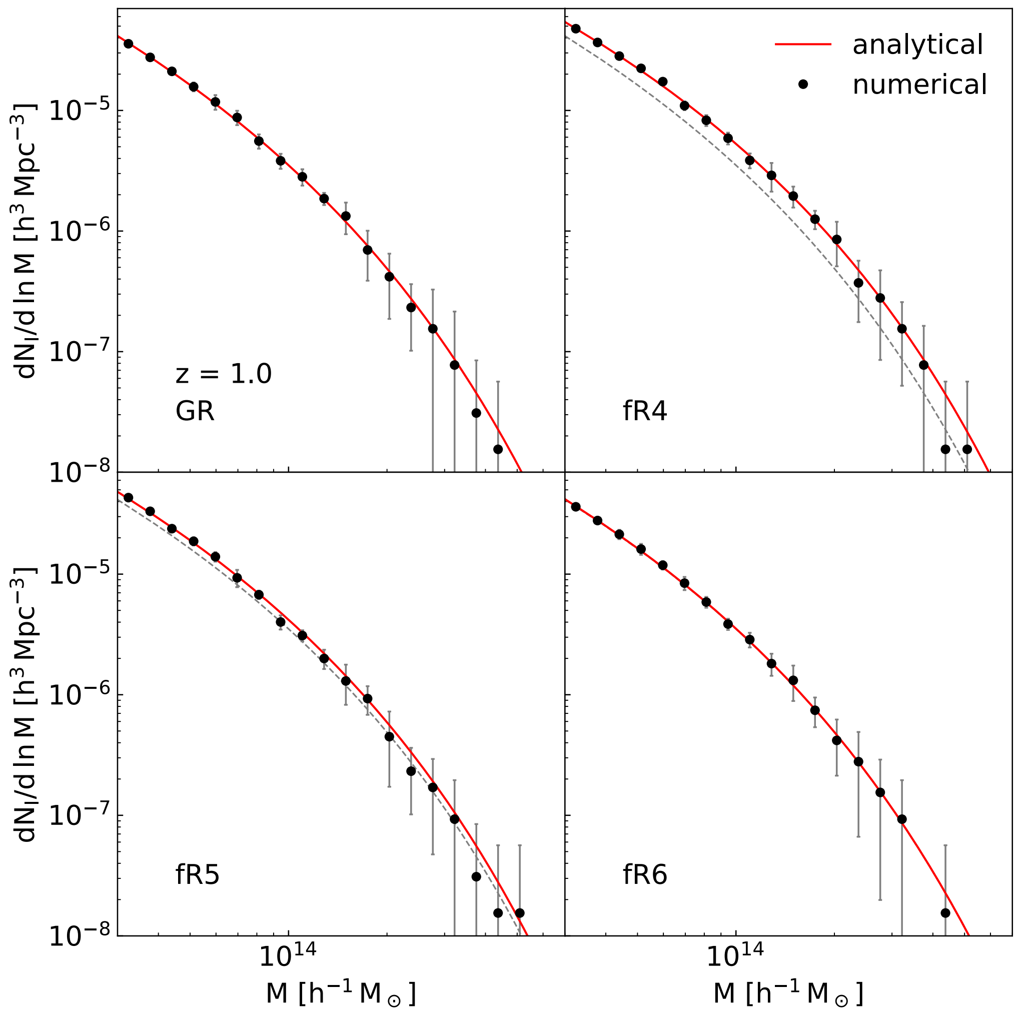

Figure 4.15. Same as Figure 4.14 but at $z = 1$.

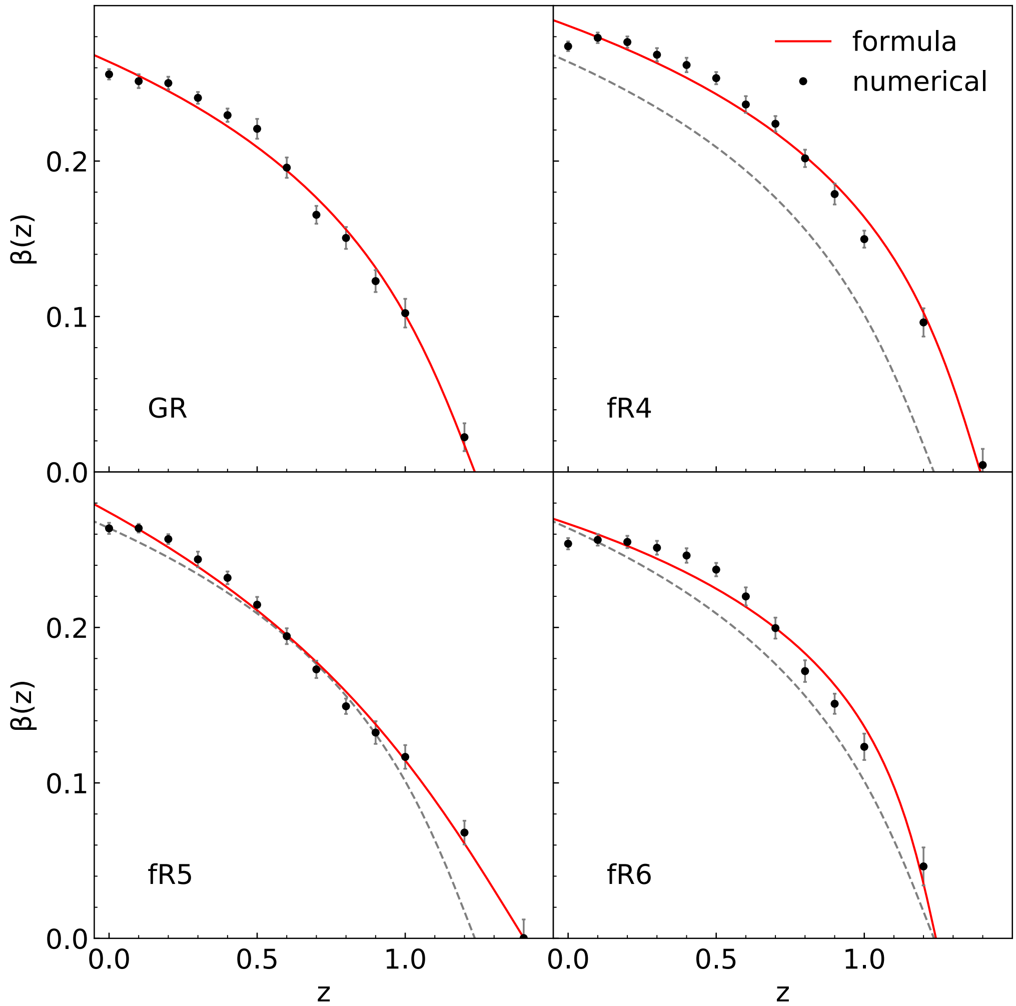

Figure 4.16. Empirically determined redshift evolution of the drifting coefficient of the field clusters (black filled circles) and fitting formula (red solid lines) for ΛCDM and three different $f(R)$ cosmologies.

$dN_{\rm I}/d\ln M$ between the GR and the fR6 cases, indicating their mutual degeneracy in the field cluster mass functions. Figure4.16 plots the redshift evolution of the drifting coefficient, $\beta(z)$ (filled black circles) as well as the fitting formula (red solid lines) and ΛCDM case comparison (grey dashed line) for the four cosmologies. As can be seen, despite that the field cluster mass functions fail to distinguish between the GR and the fR6 cases, the field cluster drifting coefficient, $\beta(z)$, can break the degeneracy, showing a substantial difference between the two cosmologies.

It is worth noting the distinct redshift dependence of the difference in $\beta(z)$ between the GR and each $f(R)$ gravity cosmology. The fR4 case yields an almost redshift-independent shift of $\beta(z)$ from that of the GR case, while the other two cases show different redshift-dependent shifts between each other. That is, for the fR5 (fR6) case, the largest deviation of $\beta(z)$ from that of the GR case occurs at the low (high) redshift ends. A qualitative explanation for this trend is provided in the following.For the fR4 case, the fifth-force is basically always unscreened at low redshifts, which implies that the haloes of all masses are equally affected by the fifth force, and that there is no sharp transition between screened and unscreened regions in the cosmic web.

Whereas, for the fR5 and fR6 cases, as the screening properties imply that the massive halos are screened, while less massive halos are not. This introduces a mass dependence in the deviation of the halo mass function from that of the GR case. In particular, for the fR6 case, the high-mass tail of the halo mass function should be almost unaffected and thus there should be an enhancement in the number of smaller-mass halos. This may have a different impact on the bias of halos at different masses, and consequently an impact on the definition of the field clusters (i.e. isolated massive objects) which could induce a different evolution of $\beta(z)$.A more quantitative analysis is required to fully understand the distinct differences in $\beta(z)$ between the GR and each $f(R)$ cosmology, which is, however, beyond the scope of this paper.

4.4 Combined Effect of $f(R)+\nu$ on $\beta(z)$

[5] Now that the validity of the analytic model of the field cluster mass function for the $f(R)$ gravity cosmology is confirmed, we repeat the whole process but for the fR4+0.3 eV, fR5+0.15 eV and fR6+0.06 eV cosmologies, which were shown to be degenerate with the GR in the standard statistics including the nonlinear density power spectrum, cluster mass functions and halo bias (Baldi et al. 2014; Giocoli et al. 2019). Figure 4.17 (Figure 4.18) depicts the same as Figure 4.14 (Figure 4.15) but for the fR4+0.3 eV, fR5+0.15 eV and fR6+0.06 eV cosmologies. As can be seen, the analytic model is still quite valid in matching the numerically obtained field cluster mass functions even for the $f(R)+\nu$ cosmologies. At $z = 0$, the three $f(R)+\nu$ cosmologies show no difference from the GR case in the field cluster mass functions. At $z = 1$, the differences in $dN_{\rm I}/d\ln M$ between the $f(R)+\nu$ and the GR cases are slightly larger but still not statistically significant. Figure 4.19 plots the same as Figure 4.16 but for the fR4+0.3 eV, fR5+0.15 eV and fR6+0.06 eV cosmologies. As can be seen, the fR4+0.3 eV cosmology yields a substantial difference in $\beta(z)$ from the GR case, in spite of their mutual degeneracy in the standard statistics. Yet, both of the fR5+0.15 eV and the fR6+0.06 eV cosmologies show almost no difference in $\beta(z)$ from the GR case.

As done in Section 4.2, we redetermine $dN_{\rm I}/d\ln M$ for both of the fR5+0.15 eV and fR6+0.06 eV cases without using prior information on the shapes of their power spectra, which are plotted in Figure 4.20. As can be seen, the analytic model, Equation (2.19), still agrees quite well with the numerically obtained field cluster mass functions for both of the cases at both of the redshifts, despite that $P(k; GR)$ is substituted for $P(k; \text{fR5}+0.15\,\text{eV})$ and $P(k; \text{fR6}+0.06\,\text{eV})$. The drifting coefficient, $\beta(z)$, redetermined without using prior information is plotted in Figure 4.21, which reveals that the three

[5] This section was published in Ryu, S., Lee, J., & Baldi, M. 2020, ApJ, 904, 93.

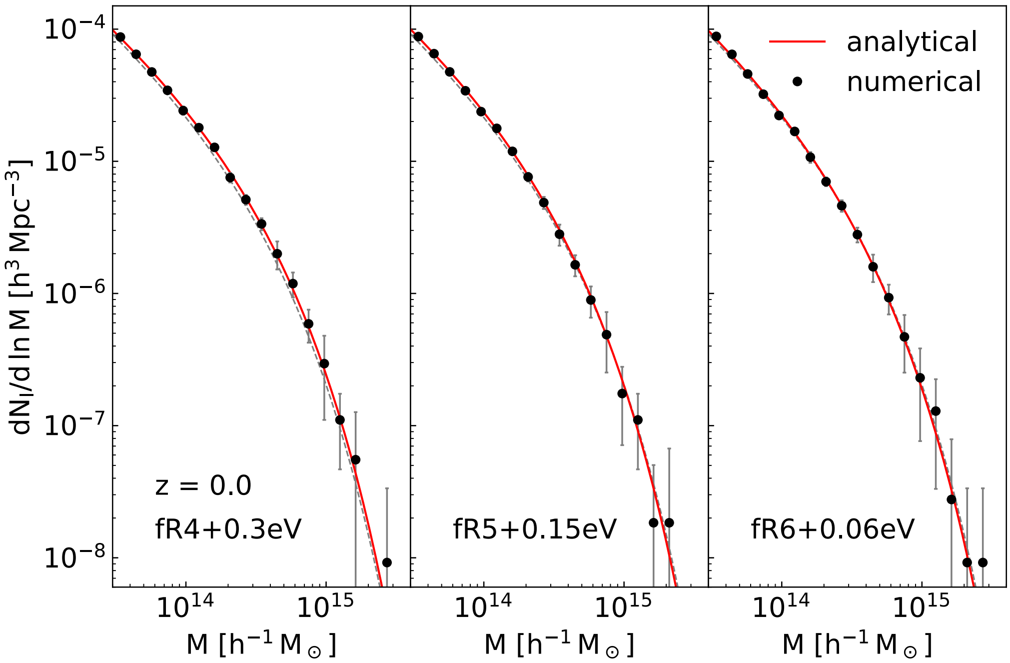

Figure 4.17. Same as Figure 4.14 but for four different $f(R)$ gravity+ν cosmologies.

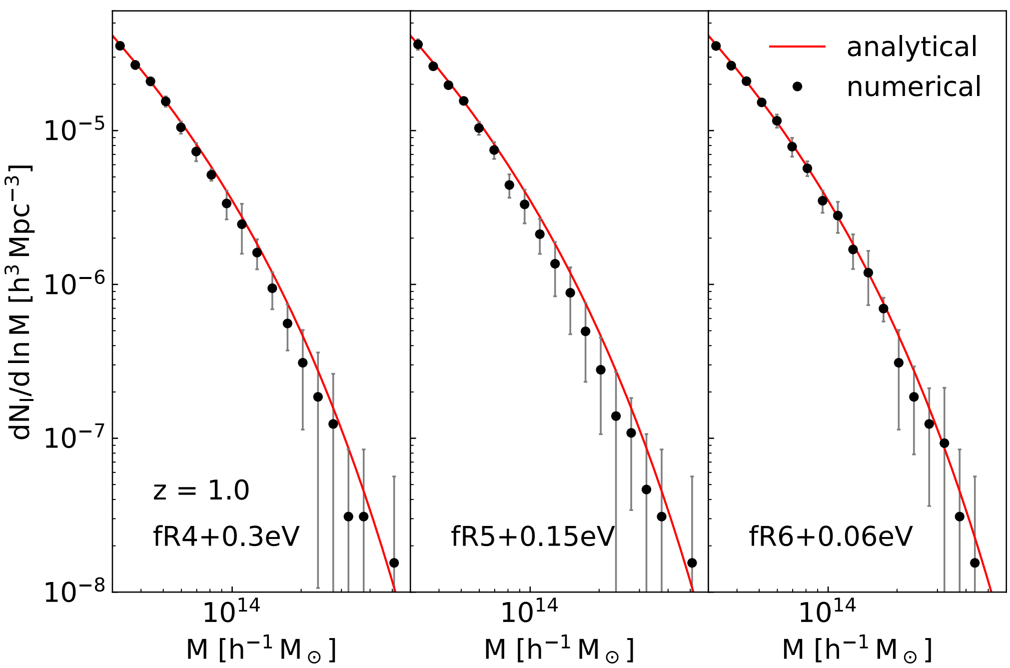

Figure 4.18. Same as Figure 4.17 at $z = 1$.

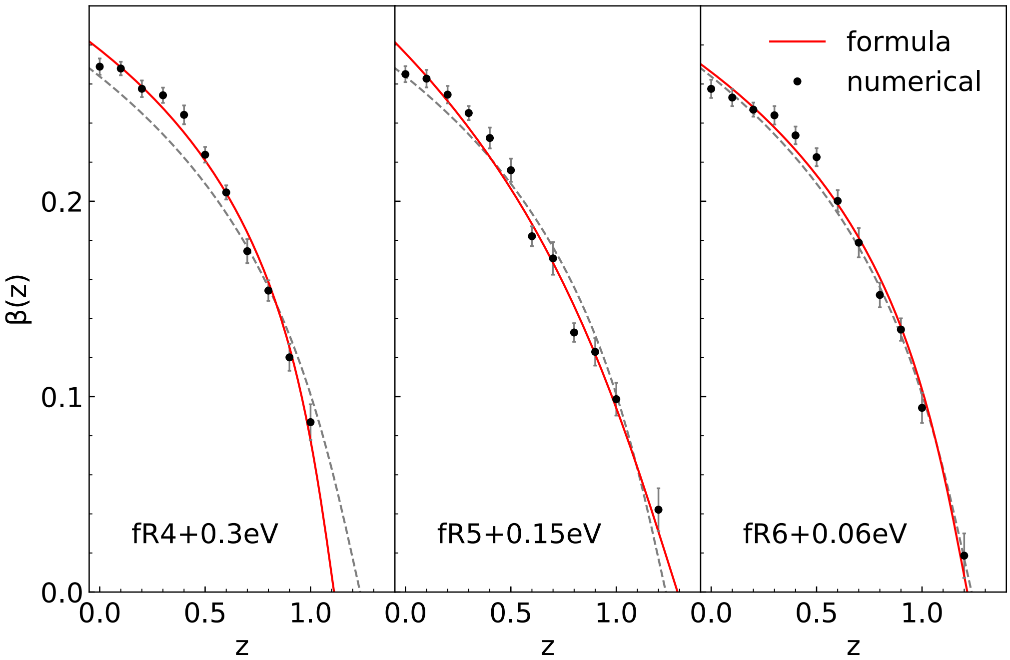

Figure 4.19. Same as Figure 4.16 but for the $f(R)$ gravity + ν cosmologies.

cosmologies yield much larger differences in $\beta(z)$.

For each cosmology, we determine the best-fit values of $\beta_A,\ q_z$ and z_c by fitting Equation (3.1) to $\beta(z)$ obtained without priors. Then, we calculate the statistical significance of the differences in the three parameters among the three cosmologies, which are shown in Figure 4.22. As can be seen, without using prior information on the linear density power spectra of the $f(R)+\nu$ cosmologies, the statistical significance of the differences in z_c between the GR and the fR5+0.15 eV and between the fR6+0.06 eV and the fR5+0.15 eV are as high as 3.48 and 3.22, respectively.

Meanwhile, for the fR6+0.06 eV case, it turns out to be not z_c but β_A that is able to distinguish it from the GR case with $\Delta\beta_A/\sigma_{\Delta\beta_A} = 2.03$. The lower statistical significance of the differences in $\beta(z)$ between the GR and the fR6+0.06 eV is likely to be at least partially due to the large errors caused by the relatively small box size of the DUSTGRAIN-pathfinder simulations. Given the distinct behaviors of $\beta(z)$ between the the GR and the fR6+0.06 eV shown in Figure 4.21, we suspect that if a halo sample from a larger simulations were used, the statistical significance would increase.The best-fit values of $\beta_A,\ q_z$ and z_c for each of the seven cosmologies simulated by the DUSTGRAIN-pathfinder are shown in Table 4.2. For the fR6+0.06 eV and fR5+0.15 eV cosmologies that are degenerate with the GR case in the standard statistics, what is listed in Table 4.2 is the best-fit values obtained without using priors in the shapes of the linear density power spectra.

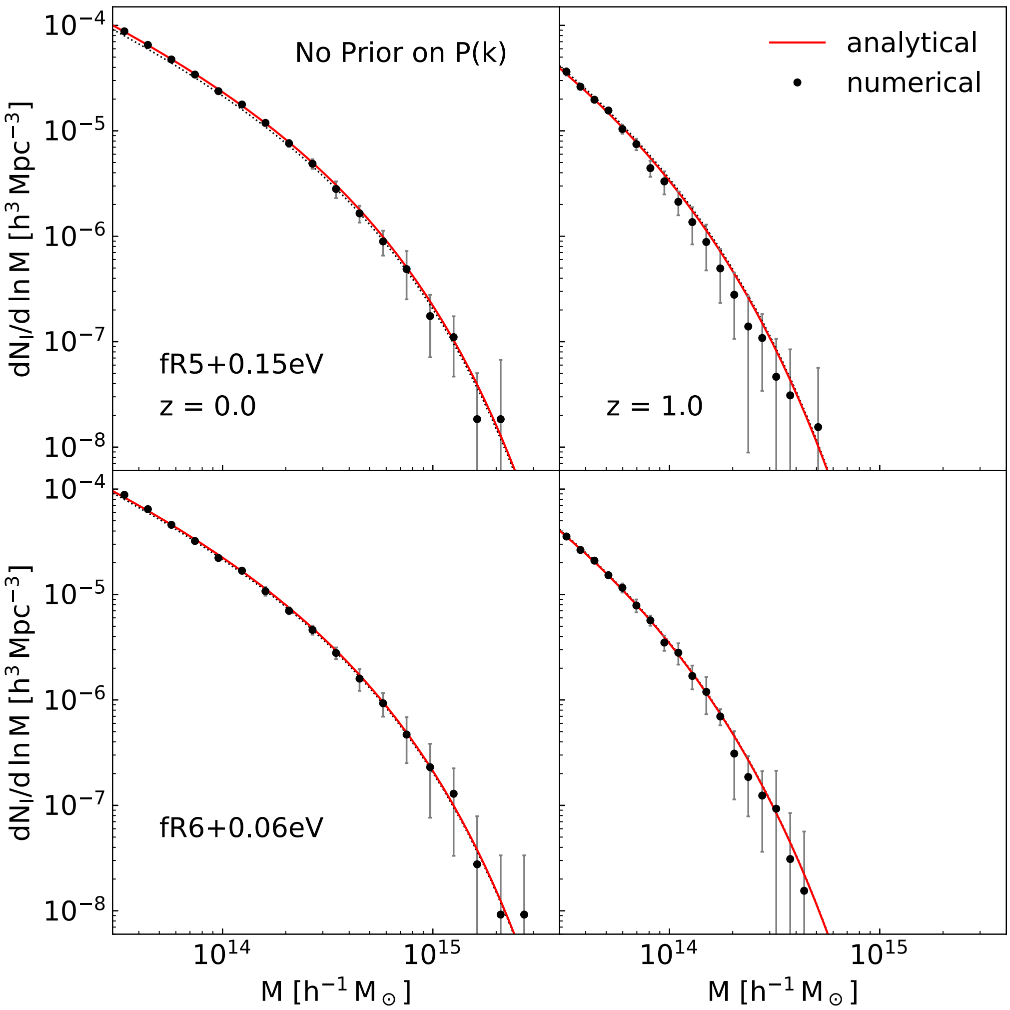

Figure 4.20. Field cluster mass functions for the fR5+0.1 eV and fR6+0.05 eV cases determined without using prior information on $P(k)$.

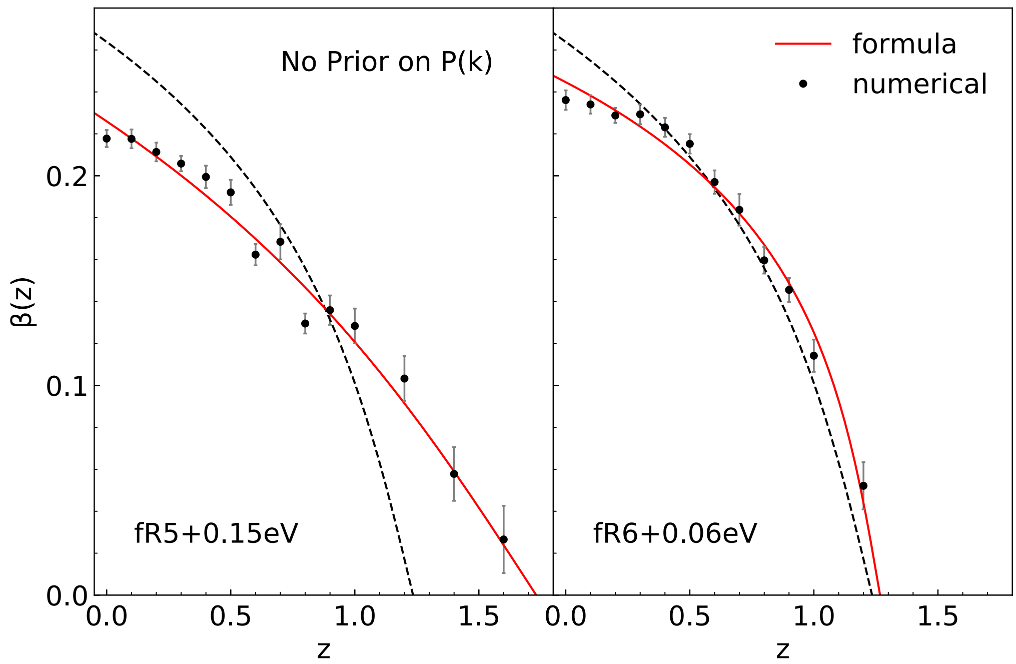

Figure 4.21. $\beta(z)$ for the fR5+0.1 eV and fR6+0.05 eV cases determined without using prior information on $P(k)$.

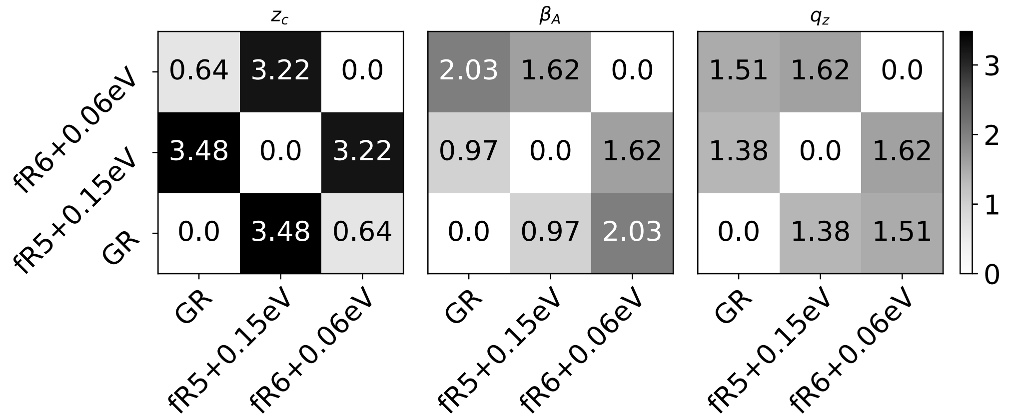

Figure 4.22. Statistical significances of the differences in z_c, β_A and q_z among the GR, fR5+0.1 eV and fR6+0.05 eV cases that are mutually degenerate in the standard diagnostics.

Chapter 5

Discussion & Conclusions

[1] Numerically determining the field cluster mass functions at various redshifts from the Mira-Titan simulations for eleven different DE cosmologies (ten different wCDM and one ΛCDM cosmologies) whose key cosmological parameters are chosen to be in the range covering well the WMAP7 constraints, we have shown that the numerical results at all redshifts for all eleven cosmologies agree very well with the analytic model obtained by Lee (2012) through a modification of the generalized excursion set formalism (Figure 3.2-3.4). The success of the analytic model has validated the key assumptions of Lee (2012) that for the field clusters the collapse barrier can be deemed deterministic and thus that their excursion set mass function can be fully characterized by a single *drifting coefficient*, β, which measures the degree of the departure of the collapse barrier height from the spherical height, δ_{sc}. It has been found that $\beta(z)$ exhibits a universal tendency of converging to zero with the increment of z and that its convergence rate as well as the value of critical redshift, z_c at which $\beta(z) = 0$ depends strongly on the background cosmology (Figures 3.5). Noting that $\beta(z)$ differs even among those

[1]This chapter was published in Ryu, S. & Lee, J. 2020, ApJ, 889, 62; Ryu, S. & Lee, J. 2020, ApJ, 894, 65; Ryu, S., Lee, J., & Baldi, M. 2020, ApJ, 904, 93.

cosmologies that are degenerate with one another in the linear power spectrum, linear growth factor and cluster mass function, we suggest that $\beta(z)$ should be in principle useful to discriminate the candidate cosmologies.

Nevertheless, since the eleven Mira-Titan cosmologies differ not only in their DE equation of states (w_0, w_a) and DE density parameters (Ω_{de}) but also in the values of the other five key cosmological parameters $(h, \Omega_m, \Omega_b, n_s, \sigma_8)$, the detected strong cosmology dependence of $\beta(z)$ cannot be entirely ascribed to the differences among the eleven models in the values of w_0, w_a and Ω_{de}. In other words, our work has demonstrated the usefulness of $\beta(z)$ as a discriminator of wCDM cosmologies from the ΛCDM model, but not as a complementary probe of DE equation of state.

A more comprehensive investigation should be carried out to sort out the sole effect of the DE equation of state on $\beta(z)$ before claiming it as a probe of DE in practice. What will be highly desirable is to examine how sensitively $\beta(z)$ reacts to the variations of the DE equation of state and density parameter by determining its shapes from a series of N-body simulations each of which has a different DE equation of state but the same values of the other key cosmological parameters. What will be even more highly desirable is to construct a theoretical formula for $\beta(z)$ from a physical principle. Although Equation (3.1) is a mere fitting formula expressed in terms of an inverse sine hyperbolic function with three adjustable parameters, its general success in matching $\beta(z)$ for all of the eleven cosmologies (Figure 3.6) hints a prospect for finding a physical formula similar to it and directly linking its three parameters to the initial conditions.

Motivated by the potential of $\beta(z)$ as a new probe of cosmology and conducting a numerical analysis of the `MassiveNuS` data (Liu et al. 2018), we have found that the massive neutrinos have a unique redshift-dependent effect on the $\beta(z)$. We have found that the presence of more massive neutrinos lowers z_c and induce a faster increase of $\beta(z)$ with the decrement of z below z_c. The $\nu\Lambda$CDM cosmology with total neutrino mass of $M_\nu = 0.6\,\mathrm{eV}$ has been found to yield higher (lower) values of β at $0 \le z \lesssim z_{\rm th}$ ($z_{\rm th} \lesssim z \le z_c$) than the ΛCDM cosmology with massless neutrinos with $z_{\rm th} \sim 0.3$. Noting that this redshift-dependent effect of massive neutrinos on β is quite unique and distinct especially from the redshift-independent effect of σ_8 on $\beta(z)$, we suggest that the drifting coefficient of the field cluster mass function should allow us to break the notorious σ_8-M_ν degeneracy, which has haunted for long the conventional probes of M_ν based on the linear density power spectrum.

Our physical explanation for this distinct redshift-dependent effect of M_ν on $\beta(z)$ is that it is generated by a competition between the suppressed small-scale powers and the increased degree of the anisotropy of the cosmic web in the presence of massive neutrinos. As shown by Bernardeau (1994), the formation of a rare event like a massive cluster (or a field cluster) is well approximated by a spherical collapse process. The rarer an object is, the more spherically its gravitational collapse proceeds. In the presence of more massive neutrinos which suppress more severely the small-scale powers, a field cluster corresponds to an even rarer object since it originates from a more extreme local maximum in the initial density field. Therefore, it is naturally expected that in the presence of more massive neutrinos the collapse density threshold δ_c for the field clusters would become closer to the spherical threshold δ_{sc} (or equivalently, β closer to zero).

The free streaming of massive neutrinos, however, has another effect of rendering the cosmic web more anisotropic in the deeply nonlinear stage. According to the previous works (e.g., Shim et al. 2014; Ho et al. 2018) which found the degree of the anisotropy of the cosmic web to depend on the background cosmology, the stronger gravity at a given scale pulls down the anisotropic feature of the cosmic web in the nonlinear stage. The free streaming of massive neutrinos plays a role along with DE in weakening the gravitational clustering on the cluster scale, which in consequence increases the degree of the anisotropy of the cosmic web. The stronger tidal influences from the more anisotropic cosmic web (Bond et al. 1996) deviate the collapse process further from the spherical symmetry, elevating β above zero.

At high redshifts ($z_{\rm th} \lesssim z \leq z_c$), the first effect of massive neutrinos overwhelms the second, lowering β close to zero, since the high-z field clusters correspond to the rarest events formed through the collapses of the highest density peaks which proceed in almost perfectly spherically. However, at lower redshifts ($0 \leq z \lesssim z_{\rm th}$) after the onset of the nonlinear evolution of the cosmic web, the second effect wins over the first, deviating β further from zero. Our result shown in Figure 4.6 reveals the M_ν-dependence of the threshold redshift, $z_{\rm th}$, at which the second effect becomes more dominant than the first. It is around 0.3 for the case of $M_\nu = 0.6\,{\rm eV}$, while it becomes around zero for the case of $M_\nu = 0.1\,{\rm eV}$. The more massive neutrinos induce the turn-over of the second effect to occur earlier. Our future work is in the direction of constructing a more theoretical model for $\beta(z)$, within which the M_ν-dependences of $z_{\rm th}$ and z_c could be predicted.

Another important hint of this work is that the sensitivity of $\beta(z)$ to M_ν might be high enough to detect the effect of massive neutrinos on it, even in case that M_ν is as low as $0.1\,{\rm eV}$ below the Planck constraint (Planck Collaboration et al. 2018). The signal of the difference in z_c between the ΛCDM and $\nu\Lambda$CDM with $M_\nu = 0.1\,{\rm eV}$ ($M_\nu = 0.6\,{\rm eV}$) cosmologies has been found to be approximately four (ten) times higher than the propagated errors. Given that the observational data from much larger volumes than that of the `MassiveNuS` are already in the pipeline (e.g., Euclid Collaboration et al. 2019), we conclude that the drifting coefficient of the field cluster mass function, $\beta(z)$, has a good prospect for providing a very powerful complementary probe of M_ν in practice.

We have also studied whether or not the $\beta(z)$ can break the degeneracy between the non-standard and the standard ΛCDM+GR cosmologies by utilizing the data from the CoDECS and DUSTGRAIN-pathfinder simulations. For this study, we have considered eleven different non-standard cosmologies which include 5 different cDE (EXP001, EXP002, EXP003, EXP008e3 and SUGRA), 3 different $f(R)$ gravity (fR4, fR5, fR6), and 3 different $f(R)$ gravity+ν cosmologies (fR4+0.3eV, fR5+0.15eV, fR6+0.06eV).

Among the cDE and $f(R)$ gravity cosmologies, the EXP001 and fR6 have been known to be very similar to the ΛCDM+GR in the linear density power spectra and cluster mass functions at $z = 0$, due to their extremely weak DM-DE coupling and fifth force, respectively. The three $f(R)$ gravity+ν cosmologies have been known to be degenerate not only with the ΛCDM+GR but also among one another in the standard diagnostics that include the cluster mass functions, halo bias, and nonlinear density power spectrum (Baldi et al. 2014; Giocoli et al. 2019). Analyzing the catalogs of the FoF bound objects for each cosmology, following findings were obtained.

- The analytic model of Lee (2012) for the field cluster mass functions agrees excellently with the numerical results at all redshifts for all of the non-standard cosmologies.

- The empirical formula for $\beta(z)$, Equation (3.1), works fairly well for all of the non-standard cosmologies.

- Despite that they produce very similar (field) cluster mass functions, the ΛCDM and the SUGRA cosmologies substantially differ in $\beta(z)$ from each other.

- The degeneracy between the ΛCDM and the EXP001 in the (field) cluster mass functions can be broken by $\beta(z)$ with 2.53σ significance without using any prior information on the linear density power spectrum, $P(k; \mathrm{EXP001})$.

- The degeneracy between the ΛCDM+GR and the fR4+0.3eV in the linear density power spectra and (field) cluster mass functions can be broken by $\beta(z)$ with high statistical significance.

- The degeneracy among the ΛCDM+GR, fR5+0.15eV and fR6+0.05eV cosmologies in the standard diagnostics can be broken by $\beta(z)$ with minimum 2.01σ significance, without using any prior information on the linear density power spectra.

To understand the advantage of using $\beta(z)$ as a cosmology discriminator, it may be worth comparing $\beta(z)$ with the standard diagnostics such as the linear density power spectrum, nonlinear density bi spectrum and cluster mass function. As for the linear density power spectrum, it deals with isotropically averaged densities and thus fail to capture independent information contained in the anisotropic nonlinear cosmic web about the background cosmology (Naidoo et al. 2020). As for the nonlinear density bi spectrum that treats the nonlinear anisotropic density field, it is not readily observable, suffering from highly nonlinear halo bias and redshift space distortion effects. Regarding the cluster mass function, although it is free from the halo bias and redshift space distortion effect, it varies most sensitively with the value of σ_8. If two different cosmologies share an identical value of σ_8 (e.g., ΛCDM and SUGRA), the cluster mass function is apt to fail in telling them apart.

Meanwhile, the field cluster drifting coefficient, $\beta(z)$, deals with the non-spherical collapse occurring in the anisotropic cosmic web that contains additional information on the initial conditions. It is free from the halo bias and redshift space distortion effect, directly quantifying how the background cosmology deviates from the Einstein-de Sitter state which sensitively depends on the evolution of the energy contents of the universe. Notwithstanding, we have yet to find a direct link of $\beta(z)$ to the initial conditions, which weakens its power as a probe of gravity and dark sector physics. The very fact that the inverse sine hyperbolic function provides a fairly good approximation to the empirically determined $\beta(z)$ for all of the cosmologies hints that it should be beyond a mere fitting formula. Our future work is in the direction of theoretically deriving $\beta(z)$ from first principles, providing a physical explanation for why $\beta(z)$ behaves as an inverse sine hyperbolic function of z and establishing its direct link to the initial conditions.

Another advantage is high observational applicability of $\beta(z)$. As shown in Figure 4.21, the fR5+0.15eV and fR6+0.06eV cases substantially differ from the GR case in the low-z values of $\beta(z)$ ($z < 0.5$). In other words, it does not require a large sample of the high-z clusters with $z > 0.5$ to distinguish between the $f(R)+\nu$ and the GR cases with $\beta(z)$ in practice. Yet, to distinguish between the fR5+0.15eV and the fR6+0.06eV cases as well as between the $f(R)$ gravity and the cDE cosmologies with $\beta(z)$, it indeed requires a large cluster sample from a wide range of redshifts. The upcoming large-scale deep surveys such as the LSST (Large Synoptic Survey Telescope) or EUCLID that is expected to cover the redshift range up to $z \sim 2$ (Tyson 2002; Amendola et al. 2013) will improve prospects for $\beta(z)$ as a cosmological discriminator.

Bibliography

Achitouv, I., Wagner, C., Weller, J., et al. 2014, JCAP, 2014, 077

Amendola, L. 2000, Phys. Rev. D, 62, 043511

Amendola, L. 2004, Phys. Rev. D, 69, 103524

Amendola, L., Appleby, S., Bacon, D., et al. 2013, Living Reviews in Relativity, 16, 6

Baldi, M., Pettorino, V., Robbers, G., et al. 2010, MNRAS, 403, 1684

Baldi, M. 2012a, MNRAS, 420, 430

Baldi, M. 2012b, MNRAS, 422, 1028

Baldi, M., Villaescusa-Navarro, F., Viel, M., et al. 2014, MNRAS, 440, 75

Basilakos, S., Plionis, M., & Lima, J. A. S. 2010, Phys. Rev. D, 82, 083517

Behroozi, P. S., Wechsler, R. H., & Wu, H.-Y. 2013, ApJ, 762, 109

Bernardeau, F. 1994, ApJ, 427, 51

Benson, B. A., de Haan, T., Dudley, J. P., et al. 2013, ApJ, 763, 147

Biswas, R., Heitmann, K., Habib, S., et al. 2019, arXiv e-prints, arXiv:1901.10690

Bond, J. R., Kofman, L., & Pogosyan, D. 1996, Nature, 380, 603

Bond, J. R., & Myers, S. T. 1996, ApJS, 103, 1

Buchdahl, H. A. 1970, MNRAS, 150, 1

Castorina, E., Sefusatti, E., Sheth, R. K., et al. 2014, JCAP, 02, 049

Chevallier, M., & Polarski, D. 2001, International Journal of Modern Physics D, 10, 213

Chiueh, T., & Lee, J. 2001, ApJ, 555, 83

Choudhury, S. R., & Choubey, S. 2018, JCAP, 2018, 017

Choudhury, S. R., & Hannestad, S. 2019, JCAP, 07, 037

Clifton, T., Ferreira, P. G., Padilla, A., et al. 2012, Phys. Rep., 513, 1

Corasaniti, P. S. & Achitouv, I. 2011a, Phys. Rev. Lett., 106, 241302

Corasaniti, P. S. & Achitouv, I. 2011b, Phys. Rev. D, 84, 023009

Costanzi, M., Villaescusa-Navarro, F., Viel, M., et al. 2013, JCAP, 2013, 012

Di Valentino, E., Melchiorri, A., Mena, O., et al. 2020, Physics of the Dark Universe, 30, 100666

Eke, V. R., Cole, S., & Frenk, C. S. 1996, MNRAS, 282, 263

Euclid Collaboration, Blanchard, A., Camera, S., et al. 2019, arXiv e-prints, arXiv:1910.09273

Fan, X., Bahcall, N. A., & Cen, R. 1997, ApJ, 490, L123

García-Farieta, J. E., Marulli, F., Veropalumbo, A., et al. 2019, MNRAS, 488, 1987

Giusarma, E., Gerbino, M., Mena, O., et al. 2016, Phys. Rev. D, 94, 083522

Giusarma, E., Vagnozzi, S., Ho, S., et al. 2018, Phys. Rev. D, 98, 123526

Giocoli, C., M., Baldi, M., & Moscardini, L. 2018, MNRAS, 481, 2813

Gunn, J. E., & Gott, J. R. 1972, ApJ, 176, 1

Habib, S., Pope, A., Finkel, H., et al. 2016, New Astronomy, 42, 49

Hagstotz, S., Costanzi, M., Baldi, M., et al. 2019, MNRAS, 486, 3927

Heitmann, K., Higdon, D., White, M., et al. 2009, ApJ, 705, 156

Heitmann, K., Bingham, D., Lawrence, E., et al. 2016, ApJ, 820, 108

Heitmann, K., Uram, T. D., Finkel, H., et al. 2019, ApJS, 244, 17

Ho, A., Gronke, M., Falck, B., et al. 2018, A&A, 619, A122

Hojjati, A., Pogosian, L. & Zhao, G. 2011, JCAP, 08, 005

Hu, W., & Sawicki, I. 2007, Phys. Rev. D, 76, 064004

Ichiki, K., & Takada, M. 2012, Phys. Rev. D, 85, 063521

Komatsu, E., Smith, K. M., Dunkley, J., et al. 2011, ApJS, 192, 18

Lacey, C., Cole, S. 2017, MNRAS, 271, 676

Lahav, O., Lilje, P. B., Primack, J. R., Rees, M. J. 1991, MNRAS, 251, 128

Lawrence, E., Heitmann, K., Kwan, J., et al. 2017, ApJ, 847, 50

Lee, J. 2012, ApJ, 752, 40

Lewis, A., Challinor, A., & Lasenby, A. 2000, ApJ, 538, 473

Li, B., & Barrow, J. D. 2007, Phys. Rev. D, 75, 084010

Linder, E. V. 2003, Phys. Rev. Lett., 90, 091301

Liu, J., Bird, S., Zorrilla Matilla, J. M., et al. 2018, JCAP, 03, 049

Naidoo, K., Whiteway, L., Massara, E., et al. 2020, MNRAS, 491, 1709

Macciò, A. V., Quercellini, C., Mainini, R., et al. 2004, Phys. Rev. D, 69, 123516

Maggiore, M., & Riotto, A. 2010a, ApJ, 711, 907

Maggiore, M., & Riotto, A. 2010b, ApJ, 717, 515

Mainini, R., & Bonometto, S. 2006, Phys. Rev. D, 74, 043504

Mangano, G., Miele, G., & Pettorino, V. 2003, Modern Physics Letters A, 18, 831

Marulli, F., Carbone, C., Viel, M., et al. 2011, MNRAS, 418, 346

Merten, J., Giocoli, C., Baldi, M., et al. 2019, MNRAS, 487, 104

Pace, F., Waizmann, J. C., & Bartelmann, M. 2010, MNRAS, 406, 1865

Peel, A., Pettorino, V., Giocoli, C., et al. 2018, A&A, 619, A38

Peel, A., Lalande, F., Stark, J.-L., et al. 2018, Phys. Rev. D, 100, 023508

Pettorino, V., & Baccigalupi, C. 2008, Phys. Rev. D, 77, 103003

Planck Collaboration, Ade, P. A. R., Aghanim, N., et al. 2014, A&A, 571, A20

Planck Collaboration, Ade, P. A. R., Aghanim, N., et al. 2016, A&A, 594, A24

Planck Collaboration, Aghanim, N., Akrami, Y., et al. 2018, arXiv e-prints, arXiv:1807.06209

Press, W. H., & Schechter, P. 1974, ApJ, 187, 425

Puchwein, E., Baldi, M., & Springel, V. 2013, MNRAS, 436, 348

Reed, D., Gardner, J., Quinn, T., et al. 2003, MNRAS, 346, 565

Robertson, B. E., Kravtsov, A. V., Tinker, J., et al. 2009, ApJ, 696, 636

Sheth, R. K., Mo, H. J., & Tormen, G. 2001, MNRAS, 323, 1

Sheth, R. K., & Tormen, G. 2002, MNRAS, 329, 61

Shim, J. & Lee, J. 2013, ApJ, 777, 74

Shim, J., Lee, J., & Li, B. 2014, ApJ, 784, 84

Springel, V., White, S. D. M., Tormen, G., et al. 2001, MNRAS, 328, 726

Springel, V. 2005, MNRAS, 364, 1105

Starobinsky, A. A. 1980, Phys. Rev. B, 91, 99

Tinker, J., Kravtsov, A. V., Klypin, A., et al. 2008, ApJ, 688, 709

Tyson, J. A. 2002, Proc. SPIE, 4836, 10

Vagnozzi, S., Giusarma, E., Mena, O., et al. 2017, Phys. Rev. D, 96, 123503

Viel, M., Haehnelt, M. G., & Springel, V. 2010, JCAP, 06, 015

Vikhlinin, A., Kravtsov, A. V., Burenin, R. A., et al. 2009, ApJ, 692, 1060

Villaescusa-Navarro, F., Bird, S., Peña-Garay, C., et al. 2013, JCAP, 03, 019

Virtanen, P. et al. 2020, Nature Methods, 17, 261

Wang, L., & Steinhardt, P. J. 1998, ApJ, 508, 483

Warren, M. S., Abazajian, K., Holz, D. E., et al. 2006, ApJ, 646, 881

Wetterich, C. 1995, A&A, 301, 321

Wintergerst, N., & Pettorino, V. 2010, Phys. Rev. D, 82, 103516

Wright, B. S., Koyama, K., Winther, H. A., et al. 2019, JCAP, 06, 040

Zhao, G., Pogosian, L., Silvestri, A., et al. 2009, Phys. Rev. D, 79, 083513

Zucca, A., Pogosian, L., Silvestri, A., et al. 2019, JCAP, 05, 001

요 약

초은하단에 속한 은하단은 주변과의 중력적 상호작용에 의해 분산된 붕괴 밀도 장벽 δ_c를 갖는다. 이와 반대로, 저밀도 지역에 위치한 고립은하단은 하나의 값으로 결정된 δ_c를 보인다. 이 연구는 Mira-Titan(역동적 암흑에너지 모형)과 CoDECS(물질과 엮인 암흑에너지 모형) 시뮬레이션 데이터를 분석하여 비표준 암흑에너지 모델에서의 결정적 δ_c의 진화를 분석한다. 또한, Cosmological Massive Neutrino(질량을 가진 중성미자 모형)과 DUSTGRAIN-*pathfinder*($f(R)$ 중력, 질량을 가진 중성미자와 $f(R)$ 중력 혼합 모형) 시뮬레이션 데이터를 분석하여 다양한 비표준 우주론 모형에서의 δ_c를 탐구한다. 먼저 각 우주론 모형의 고립은하단 질량함수를 여러 적색편이에서 수치적으로 계산한다. 이 후, 얻어진 수치적 질량함수에 단일 변수로 매개되는 해석적 모형을 피팅하여 붕괴 밀도 장벽의 아인슈타인-디시터 우주에서의 값 ($\delta_{sc} = 1.686$) 과의 편차를 수치화하는 해석적 모형의 단일 변수 β (표류계수)를 얻어낸다. 결과적으로 모든 우주론, 모든 적색편이에서 피팅된 해석적 모형이 수치적 질량함수와 훌륭히 일치하였다. 또한 배경 우주론과 무관하게 $\beta(z)$는 보편적인 경향성을 보였는데, $z = 0$에서 양의 값을 가졌으며 적색편이가 증가하고 암흑에너지의 영향이 감소함에 따라 점진적으로 감소하여 0에 수렴하였다. $\beta(z)$ 가 0으로 수렴하는 임계 적색편이 z_c가 각기 다른 우주론마다 현저히 다른 값을 가졌으며, δ_c가 거의 동일한 파워스팩트럼($P(k,z)$)과 질량함수를 갖는 여러 축퇴된 우주론을 구분해낼 수 있음을 보였다. 따라서 $\beta(z)$로 수치화되는 구형대칭 붕괴로부터 벗어난 정도의 진화는 강력한 우주론의 탐사 도구가 될 수 있을 예견된다.

주요어: 우주거대구조 – 우주론 모형

학 번: 2020-25868

감 사 의 글

짧은 지난 2년간 많은 사람의 도움 아래 정말 많은 우수한 연구를 수행할 수 있었습니다. 이 논문이 작성될 수 있게 언제나 저의 주변에서 도움을 주신 분께 감사한 마음을 전하고자 감사의 글을 적습니다.

지난 5학기 동안 저를 지도해주신 이정훈 지도교수님, 교수님이 계셨기에 제 모든 연구가 있을 수 있었습니다. 언제나 더 편하고 쾌적한 환경에서 연구를 수행할 수 있도록 지원을 아끼지 않으시고, 어려움과 부족함 없이 생활할 수 있도록 도움을 주셨습니다. 좋은 연구를 수행할 수 있도록 이끌어주심과 동시에 좋은 연구자로 성장할 수 있도록 진심 어린 관심과 애정을 주셨기에 여러 우여곡절도 어려운 일도 있었지만 여기까지 올 수 있었습니다. 정말 감사합니다. 제 행복한 미래를 기원해 주셨듯 교수님께서도 항상 행복하시길 바랍니다.

제가 대학원 생활을 잘 헤쳐 나갈 수 있도록 도움을 주신 천문 가족들께도 감사합니다. 학교생활에 필요한 정보들을 물을 선배나 동기가 없는 연구실에 있어 많은 주변 다른 연구실 선배들이나 행정실 선생님들을 귀찮게 한 것 같습니다. 사소하고 바보 같은 질문들이라도 언제나 성심성의껏 답해주시고 도움이 될만한 정보들을 나눠주셨던 진선호, 이가인 선배에게 고맙다는 말을 남깁니다. 항상 번거로운 일들을 만들어내고 쉬운 일도 참 어렵게 만드는 저 이지만 언제나 최대한 도움을 주려 노력해주신 학과 행정실 노현주, 김경숙, 이효주, 원선희 선생님 감사합니다.

그리고 지난 2년간 가슴 아프고 힘든 일도 참 많았습니다. 언제나 제 뒤에서 든든한 버팀목이 되어 주시고 사랑으로 안아주신 부모님께 감사하다는 말을 전합니다. 언제나 해줄 수 있는 게 없어 미안하고 답답하다 말씀하시지만, 항상 곁에 있어 주셨기에 그냥 힘내라는 한 마디, 걱정해주시는 한 마디만으로도, 언제든 기대어 쉴 수 있는 곳이 있다는 것만으로도, 무슨 일이 있든 제 편에서 언제나 제가 더 행복한 삶을 살 수 있도록 최선을 다해주실 분이 있다는 것만으로도 제겐 가장 소중하고 감사한 두 분이십니다. 감사합니다. 사랑합니다.

마지막으로 이 논문의 심사를 위해 고생해주신 임명신, 황호성 교수님께 감사의 말씀을 남깁니다.

We acknowledge the support by Basic Science Research Program through the National Research Foundation (NRF) of Korea funded by the Ministry of Education (No.2019R1A2C1083855) and also by a research grant from the NRF to the Center for Galaxy Evolution Research (No.2017R1A5A1070354).

An award of computer time was provided by the Innovative and Novel Computational Impact on Theory and Experiment (INCITE) program. This research used resources of the Argonne Leadership Computing Facility, which is a DOE Office of Science User Facility supported under contract DE-AC02-06CH11357. This research also used resources of the Oak Ridge Leadership Computing Facility, which is a DOE Office of Science User Facility supported under Contract DE- AC05-00OR22725.

We thank the Columbia Lensing group (http://columbialensing.org) for making their suite of simulated maps available, and NSF for supporting the creation of those maps through grant AST-1210877 and XSEDE allocation AST-140041. We thank New Mexico State University (USA) and Instituto de Astrofisica de Andalucia CSIC (Spain) for hosting the Skies & Universes site for cosmological simulation products.

I am grateful to Professor Marco Baldi for collaborating with me.

2022년 7월

유수호 올림